DISEASES AND DISORDERS

Exercise mitigates flow recirculation and activates metabolic transducer SCD1 to catalyze vascular protective metabolites

Susana Cavallero[1,2]†, Mehrdad Roustaei[3]†, Sandro Satta[1,2], Jae Min Cho[1,2], Henry Phan[1], Kyung In Baek[3], Ana M. Blázquez-Medela[1,2], Sheila Gonzalez-Ramos[3], Khoa Vu[3], Seul-Ki Park[1], Tomohiro Yokota[1,2], Jennifer Sumner[4], Julia J. Mack[1], Curt D. Sigmund[5], Srinivasa T. Reddy[1,6], Rongsong Li[1,2], Tzung K. Hsiai[1,2,3]*

Exercise promotes pulsatile shear stress in the arterial circulation and ameliorates cardiometabolic diseases. However, exercise-mediated metabolic transducers for vascular protection remain under-investigated. Untargeted metabolomic analysis demonstrated that wild-type mice undergoing voluntary wheel running exercise expressed increased endothelial stearoyl-CoA desaturase 1 (SCD1) that catalyzes anti-inflammatory lipid metabolites, namely, oleic (OA) and palmitoleic acids (PA), to mitigate NF-κB–mediated inflammatory responses. In silico analysis revealed that exercise augmented time-averaged wall shear stress but mitigated flow recirculation and oscillatory shear index in the lesser curvature of the mouse aortic arch. Following exercise, endothelial *Scd1*–deleted mice (*Ldlr*$^{-/-}$ *Scd1*$^{EC-/-}$) on high-fat diet developed persistent VCAM1-positive endothelium in the lesser curvature and the descending aorta, whereas SCD1 overexpression via adenovirus transfection mitigated endoplasmic reticulum stress and inflammatory biomarkers. Single-cell transcriptomics of the aorta identified *Scd1*-positive and *Vcam1*-negative endothelial subclusters interacting with other candidate genes. Thus, exercise mitigates flow recirculation and activates endothelial SCD1 to catalyze OA and PA for vascular endothelial protection.

INTRODUCTION

The vascular endothelium is constantly exposed to hemodynamic shear stress (*1*), and blood flow imparts mechanotransduction to modulate cardiovascular development, injury, and repair (*2*). In response to cyclical cardiac contraction, blood flow is pulsatile in the arterial circulation, and pulsatile shear stress (PSS) is unidirectional and axially aligned with the flow direction. PSS promotes vascular protective mediators, including endothelial nitric oxide synthase (eNOS) and superoxide dismutase, to attenuate proinflammatory cytokines, adhesion molecules, and reduced form of nicotinamide adenine dinucleotide phosphate (NADPH) oxidase system (*3*–*6*). In contrast, disturbed flow, including oscillatory shear stress (OSS), develops at the lesser curvature of the aortic arch and arterial bifurcations. OSS is bidirectional and axially misaligned with the flow direction, activating NADPH oxidase to promote reactive oxygen species, including superoxide ($O_2^{-\cdot}$) and peroxynitrite (ONOO). OSS also induces nuclear factor κB (NF-κB) to increase inflammatory cytokines and the vascular cell adhesion molecule 1 (VCAM1) (*3*, *7*–*9*).

Physical exercise augments blood flow in the circulatory system and modulates molecular transducers to ameliorate metabolic disorders (*7*). During exercise, increased cardiac contractility and heart rate (HR) promote PSS to improve endothelial plasticity (*8*), mitigate atherogenesis (*9*, *10*), and delay cognitive aging and neurodegeneration (*11*–*14*). However, the specific exercise-activated metabolic transducers to mitigate oxidation and inflammation in the disturbed flow-prone vasculature remain under-investigated (*15*). Several mechano-sensitive molecular transducers have been reported to regulate fatty acid (FA) uptake and transport in vascular endothelium, including vascular endothelial growth factor B (*16*, *17*) and peroxisome proliferator–activated receptor γ (PPARγ) (*18*), a member of the nuclear receptor superfamily participating in the regulation of blood pressure (BP), hypertension, hyperlipidemia, and insulin sensitivity (*19*–*21*).

Stearoyl-CoA (coenzyme A) desaturase 1 (SCD1) is a key enzyme localized in the mitochondria-associated endoplasmic reticulum (ER) membranes (MAMs) (*22*), where it catalyzes the conversion of saturated FAs (SFAs) to omega 9-monounsaturated FAs (MUFAs). The principal metabolites of SCD1 are oleic acid (OA) and palmitoleic acid (PA), which are formed by desaturation of stearic and palmitic acid, respectively. The ratio of stearic acid to OA is implicated in the regulation of cell growth and differentiation through its effects on cell membrane fluidity and signal transduction (*23*). While laminar flow (steady and nonpulsatile flow) was reported to up-regulate PPARγ-dependent SCD1 expression in cultured human umbilical vein endothelial cells (*24*), we sought to demonstrate that voluntary wheel running exercise-augmented PSS mitigates flow recirculation in the lesser curvature of the aortic arch and activates endothelial SCD1 to catalyze protective metabolites.

To this end, our untargeted metabolomic analyses revealed that PSS promotes SCD1- catalyzed metabolites to down-regulate NF-κB–mediated inflammatory adhesion molecules and ER stress. Next, we developed an endothelial-specific deletion of SCD1 in a mouse model of atherosclerosis (*Ldlr*$^{-/-}$ *Scd1*$^{EC-/-}$) to undergo high-fat diet (HFD) and voluntary wheel running. We performed in silico simulation of flow recirculation in the lesser curvature of aortic arch and analyzed the transcriptomic profiles of SCD1-mediated gene clusters and anti-inflammatory metabolites. Our results indicate that exercise increases

[1]Division of Cardiology, Department of Medicine, David Geffen School of Medicine at University of California, Los Angeles, CA, USA. [2]Department of Medicine, VA Greater Los Angeles Health Care System, Los Angeles, CA, USA. [3]Department of Bioengineering, School of Engineering and Applied Science, University of California, Los Angeles, CA, USA. [4]Department of Psychology, College of Life Sciences, University of California, Los Angeles, CA, USA. [5]Department of Physiology, Medical College of Wisconsin, Milwaukee, WI, USA. [6]Department of Molecular and Medical Pharmacology, University of California, Los Angeles, CA, USA.
*Corresponding author. Email: thsiai@mednet.ucla.edu
†These authors contributed equally to this work.

time-averaged shear stress (τ_{ave}) and decreases oscillatory shear index (OSI_{ave}) at the lesser curvature, and PSS activates SCD1 as a metabolomic transducer to catalyze vascular protective metabolites for anti-inflammatory responses.

RESULTS

PSS activates endothelial SCD1 to catalyze lipid metabolites

Human aortic endothelial cells (HAECs) were exposed to a dynamic flow system that recapitulates spatial variations in arterial bifurcations or branching points (Fig. 1A) (*25*, *26*). Untargeted metabolomic analysis demonstrated that PSS (τ_{ave} = 50 dyne cm^{-2} and slew rate $\partial\tau/\partial t$ = 71 dyne cm^{-2} s^{-1} at 1 Hz) increased SCD1-catalyzed metabolite OA by 2-fold ($P < 0.01$ versus static) and OSS (OSS = 0.1 ± 4 dyne cm^{-2} at 1 Hz) by 1.3-fold ($P < 0.05$ versus static) (Fig. 1, B and C). The saturated FA (SFA) precursors, palmitic and stearic acid, were unaffected by PSS or OSS. Both metabolite heatmap and principal component analysis (PCA) revealed that PSS- and OSS-mediated metabolites were separated from the basal levels (Fig. 1, D and E). PSS further increased the production of glycolytic metabolites, including glucose-6-phosphate and fructose-6– phosphate, as previously reported (*26*). These results led us to investigate whether PSS increases endothelial SCD1 and subsequent vascular protection in mice undergoing voluntary wheel exercise.

In silico simulation of exercise-mediated shear stress to mitigate flow recirculation in the lesser curvature of the aortic arch

To demonstrate in silico analyses of exercise-mediated shear stress, we performed ultrasound to interrogate the mouse aortic arch (Fig. 2A).

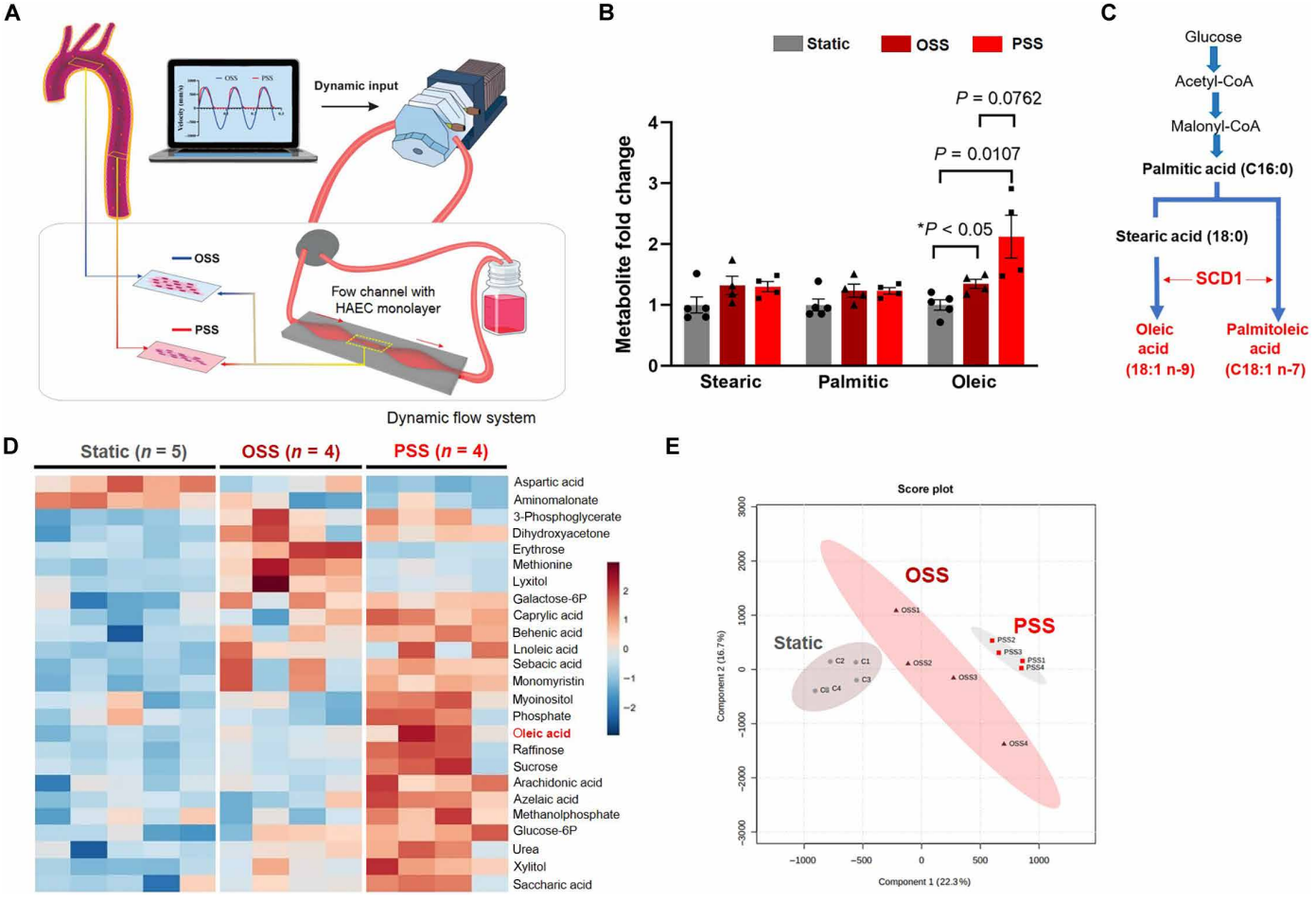

Fig. 1. PSS modulates endothelial metabolome and increases SCD1-catalyzed metabolites. (**A**) A custom-built dynamic flow system was used to simulate spatial and temporal variations in shear stress in the arterial system. The machine language (LabVIEW) drives a peristaltic pump to generate pulsatile wave forms. The configuration of the flow channel (contraction and extraction) was designed to provide the well-defined pulsatile flow with the specific slew rates ($\partial\tau/\partial t$), time-averaged shear stress (τ_{ave}), frequency [hertz (Hz)], and amplitude to simulate exercise-augmented PSS or OSS. The flow channel was maintained inside the incubator at 37°C with 5% CO_2. The confluent HAEC monolayer was seeded on the glass slides in the flow channel. (**B**) Metabolite samples were collected from HAEC lysates under the static condition (control or no flow, $n = 5$), OSS ($n = 4$), or PSS ($n = 4$ at 1 Hz for 4 hours) for the untargeted metabolic analysis. PSS or OSS significantly increased the lipid metabolite OA by 2- and 1.3-fold, respectively. (**C**) Biosynthesis of MUFA depicts that SCD1 catalyzes the rate-limiting step for the conversion of SFA (palmitic and stearic) to MUFA (palmitoleic and oleic). (**D**) The heatmap reveals an increase in both glycolytic and fatty acid metabolites. The data were analyzed after normalization and scaling using the Pareto method. (**E**) Score plots by the principal component analysis (PCA) revealed a separation of the representative endothelial metabolites. Ellipses represent 90% confidence intervals for the PSS, OSS, and static groups, respectively.

Electrocardiogram (ECG)–gated pulsed wave (PW) Doppler allowed for characterizing the time-dependent inlet flow velocity (Fig. 2C), which were calibrated for the exercise condition (*27*, *28*). The B-mode ultrasound delineated the aortic arch, and the three-element Windkessel model simulated the outlet boundary conditions for the brachiocephalic, left common carotid, left subclavian arteries, and descending aorta, respectively (Fig. 2B) (*29*). In silico analysis was accomplished by four-dimensional (4D) (space + time) computational fluid dynamics (CFD) simulation to recapitulate the velocity-colored streamlines throughout a cardiac cycle (Fig. 2E), magnitude of peak velocity profile proximal to the greater curvature, and time-averaged wall shear stress (TAWSS or τ_{ave}) at the lesser curvature of the aortic arch. Our CFD model demonstrated a low TAWSS and flow recirculation at the lesser curvature (dotted square boxes) (Fig. 2E).

To compute exercise-mediated PSS versus OSS, we incorporated changes in the HR and blood flow. Our in silico analysis demonstrated that exercise-augmented PSS increased TAWSS in both the lesser and greater curvature and mitigated flow recirculation in the lesser curvature with a small reduction in the OSI_{ave} (Fig. 2G and fig. S1). Thus, in silico analyses support that exercise modulates both TAWSS and OSI_{ave} to mitigate flow recirculation in the disturbed flow-prone lesser curvature of the aortic arch.

Exercise-augmented PSS activates endothelial SCD1 to catalyze lipid metabolites

To demonstrate exercise-mediated metabolites, we performed untargeted metabolomic analysis from male wild-type C57BL/6J mice before and immediately following 24 hours of voluntary wheel running

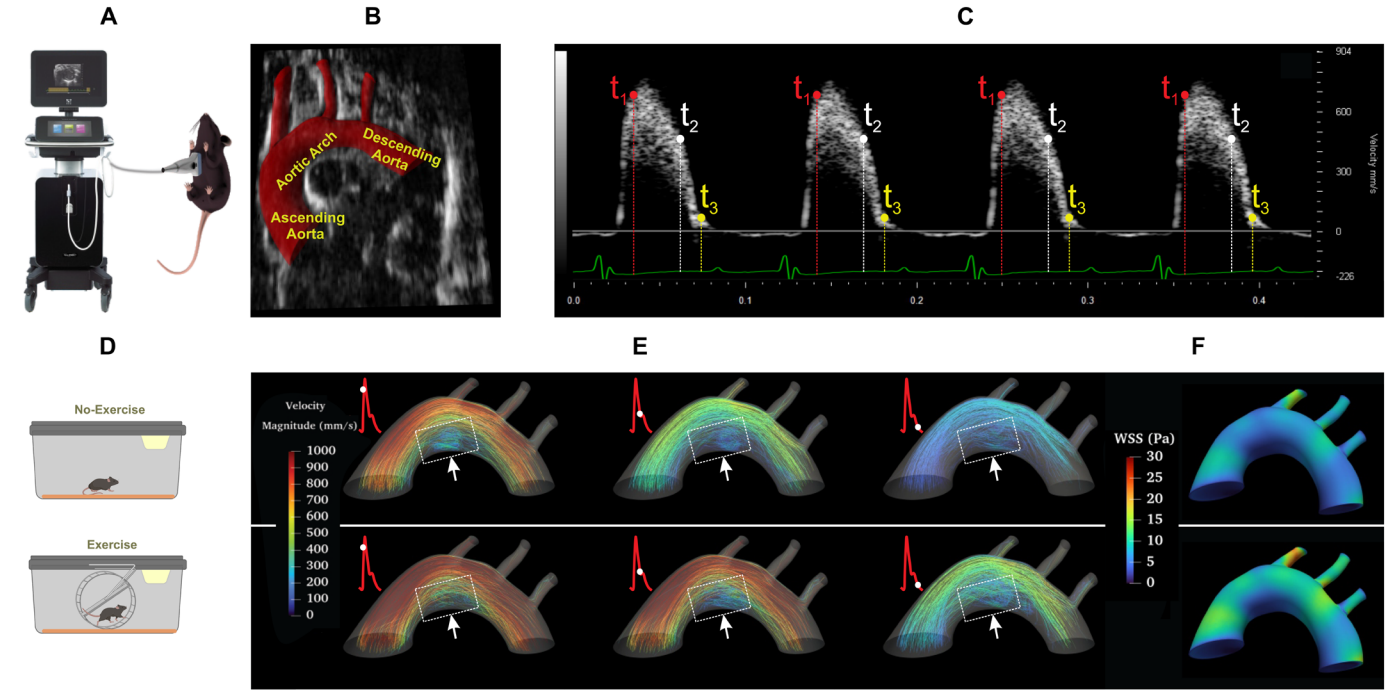

G

	Ascending Aorta	Lesser Curvature	Descending Aorta	Greater Curvature
$OSI_{Average}$				
No Exercise	0.043	0.308	0.147	0.009
Exercise	0.024	0.306	0.121	0.003
TAWSS (Pa)				
No Exercise	6.12	3.63	6.17	7.32
Exercise	7.89	4.49	7.94	10.09

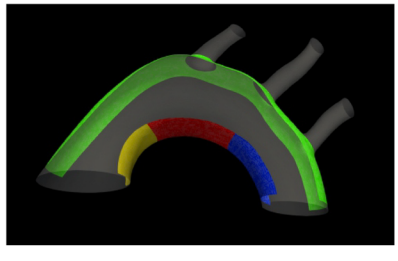

Fig. 2. In silico analysis of exercise-augmented PSS. Four-dimensional (4D) computational fluid dynamics (CFD) simulation was performed to analyze hemodynamic profiles in the mouse aorta in response to exercise. (**A**) A schematic of ultrasound system that acquired B-mode and PW Doppler images from the anesthetized mouse. (**B**) A representative B-mode image and segmentation of the mouse aortic arch and the three branches, and the descending aorta. (**C**) PW Doppler measurement was acquired from the mouse ascending aorta over four electrocardiogram (ECG)–gated cardiac cycles. (**D**) Schematics of mice in sedentary condition and engaging in voluntary wheel running. (**E**) Velocity-colored streamlines along the aortic arch demonstrating disturbed flow developed at the lesser curvature, whereas exercise-augmented shear stress mitigates flow recirculation at the disturbed flow-prone lesser curvature. (**F**) Time-averaged wall shear stress (TAWSS) over several cardiac cycles was computed and compared between no exercise and voluntary wheel running. Note that PSS develops at the greater curvature of the aortic arch and descending aorta, whereas disturbed flow, including OSS, develops at the lesser curvature. (**G**) OSI_{ave} (averaged over surface) and TAWSS are compared between lesser curvature (ascending aorta, aortic arch, and descending aorta) and greater curvature. Exercise-augmented PSS mitigates disturbed flow developed at the lesser curvature and increases TAWSS in the aortic arch. OSI, oscillatory shear index; Re, Reynolds number.

(Fig. 3, A and B). Plasma OA was significantly increased after exercise, and PA exhibited a trend to increase (Fig. 3, C and E). Saturated palmitic and stearic acids were unchanged (Fig. 3D). PCA demonstrated a distinct separation of lipid metabolites before and after exercise (Fig. 3F). In addition, an increase in succinate and oxalate was consistent with a previous report (fig. S2A) (*15*).

After 2 weeks of voluntary wheel running, en face immunostaining of the aortic endothelium demonstrated an increase in SCD1 expression in both the lesser curvature of the aortic arch (Fig. 4, B and C) and the descending aorta (Fig 4, B and D). SCD1 staining was prominent in the subcellular perinuclear area, consistent with the reported ER region (*22*), whereas SCD1 staining was absent in the endothelial-specific

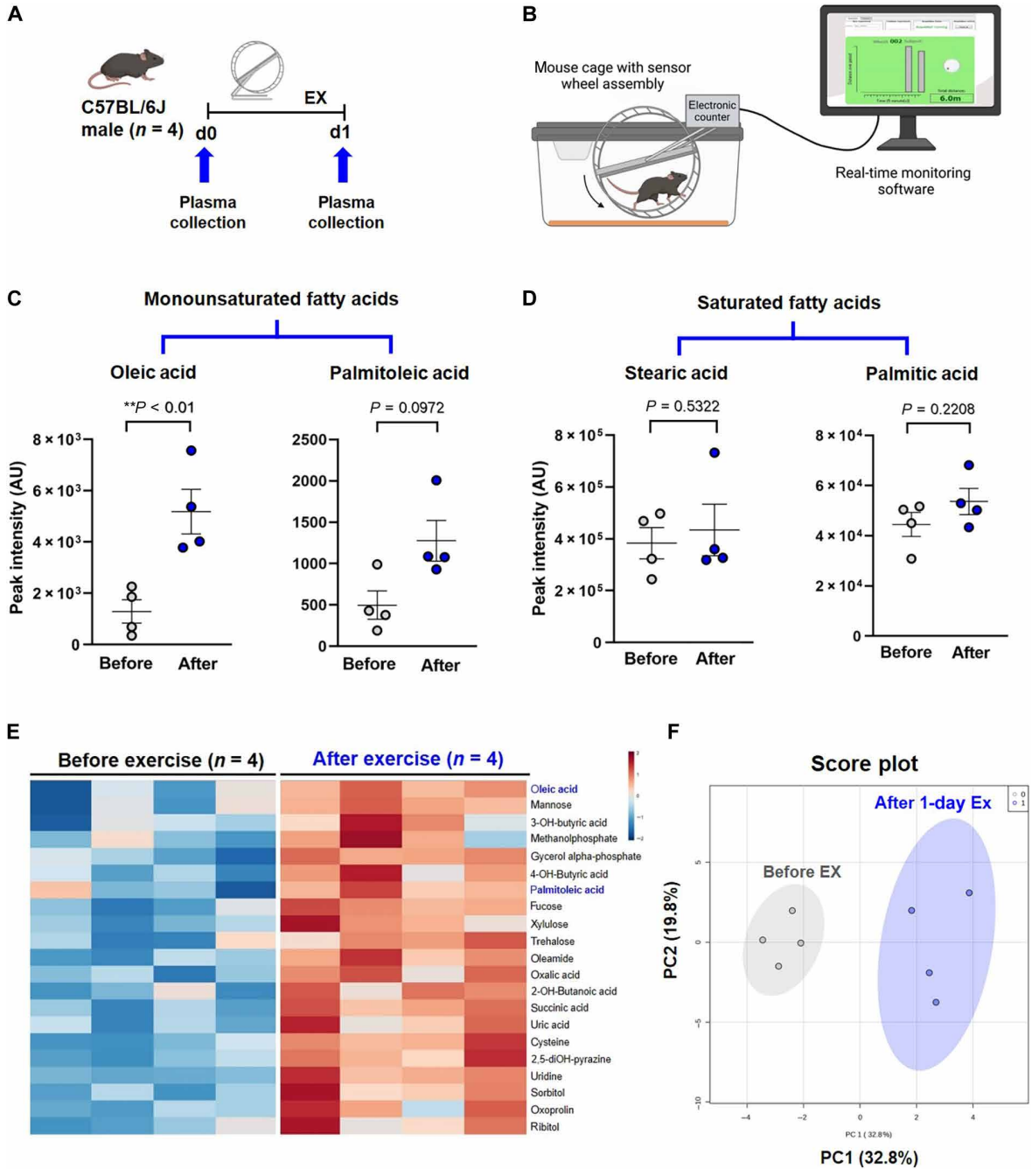

Fig. 3. Exercise alters catalysis of lipid metabolites. (**A**) A schematic representation of the animal exercise (EX) protocol. Plasma was collected from the wild-type male C57BL/6J before and after 24 hours of voluntary wheel running for metabolomic analysis ($n = 4$ male mice for each group). d, day. (**B**) The voluntary wheel running system provided real-time monitoring of rodent running activity (figure generated with Biorender.com). (**C**) Twenty-four hours of exercise increased OA and PA; however, the latter did not reach statistical significance (OA: $^{**}P < 0.01$ versus before exercise, paired *t* test, $n = 4$). (**D**) Exercise did not change the plasma levels of SFA stearic and palmitic acid. AU, arbitrary units. (**E**) Heatmap of plasma metabolites before and after exercise reveals that OA was elevated in all four mice after normalization and scaling using the Pareto method. (**F**) Score plots by the PCA support the 90% confidence intervals before and after exercise. PC, principal component.

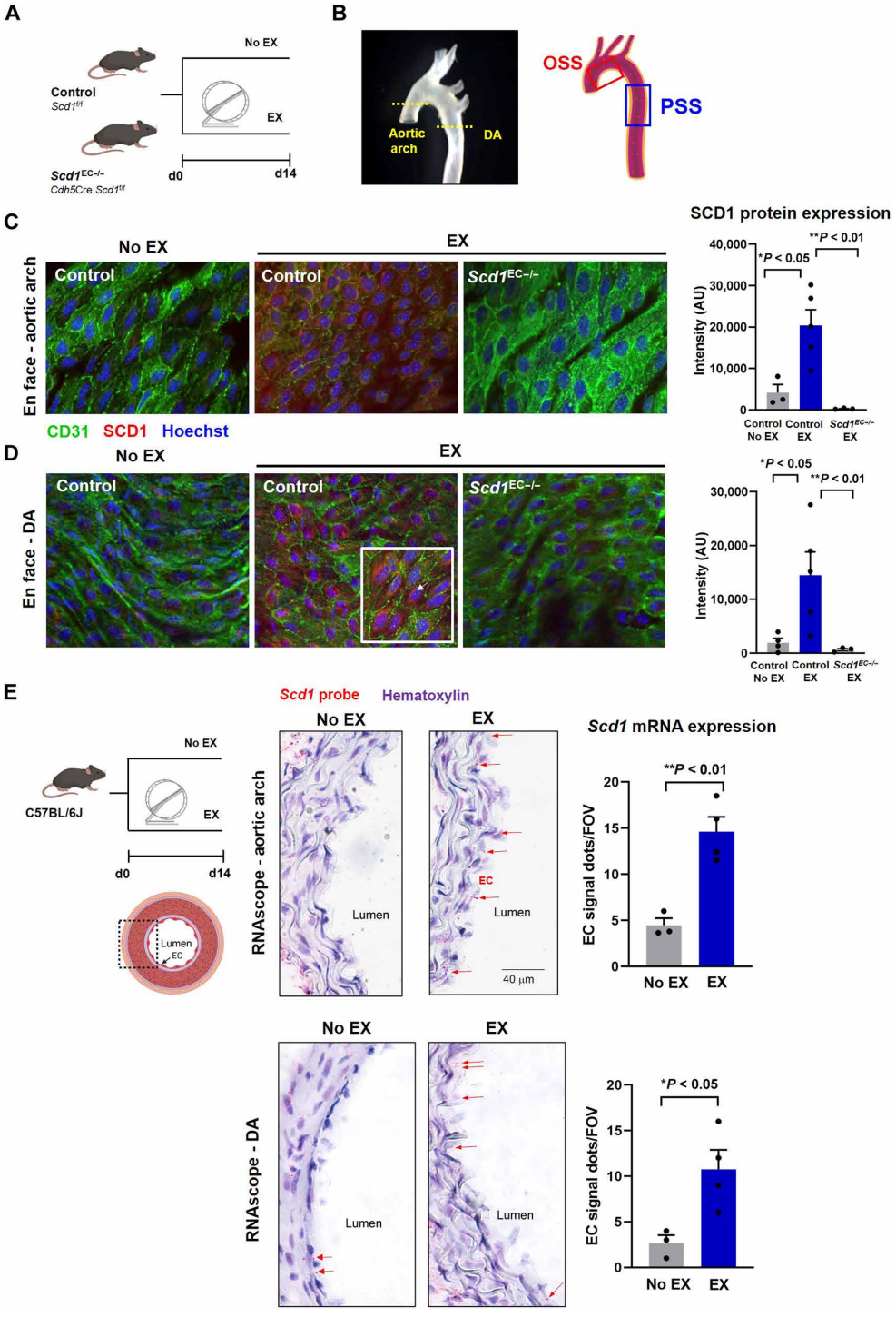

Fig. 4. Exercise activates endothelial SCD1. (**A**) Endothelial-specific *Scd1*-deleted mice underwent 14-day voluntary wheel running protocol. (**B**) En face immunofluorescence was imaged by confocal microscope at the level of the aortic arch versus descending aorta (DA). (**C** and **D**) En face immunostaining of the exposed aortic endothelium reveals that exercise increased SCD1 expression (red) in aortic endothelial cells (green, $CD31^+$) in the aortic arch (C) and the DA (D) (No EX, $n = 4$; and EX, $n = 5$; $^*P < 0.05$ versus No EX). At a higher magnification image (×63; bottom right corner inset), SCD1 staining is perinuclearly located (arrows). No SCD1 staining was observed in the $Scd1^{EC-/-}$ mice undergoing exercise in both aortic arch and DA regions. (**E**) Wild-type C57/BL6J mice underwent 14-day voluntary wheel running protocol. The *Scd1*-specific probe (RNAscope) in transversal aortic sections demonstrates prominent endothelial staining following 14 days of exercise-induced PSS both in the flow-disturbed aortic arch and the DA. Red dots (arrows) indicate the mRNA molecules in the intima layer. *Scd1*-positive signals were also present in some smooth muscle cells and periaortic adventitia (adv) in both groups. Microphotographs were taken at ×63 magnification. Quantification is shown on the right panels as the number of positive red dots in the endothelial layer averaged from 5 to 10 microscopic fields per animal (No EX, $n = 3$; and EX, $n = 4$; $^*P < 0.05$ and $^{**}P < 0.01$ versus No EX). FOV, field of view; AU, arbitrary units.

deletion of SCD1 ($Scd1^{EC-/-}$) mice. In situ hybridization (RNAscope) with an *Scd1*-specific probe corroborated increased endothelial SCD1 expression in the aortic arch and descending aorta in wild-type mice following exercise (Fig. 4E) (refer to fig. S2B and table S1 for body weight and exercise duration). Together, exercise-augmented PSS is implicated in activating endothelial SCD1 expression.

The SCD1 product OA confers inflammatory responses in endothelium

To demonstrate the role of SCD1-mediated metabolites for vascular endothelial protection, we assessed the atherogenic inflammatory markers (*30*–*32*). OA treatment reduced lipopolysaccharide (LPS)–induced *Vcam1*, *Icam1*, *Mcp1*, *Esel* (E-selectin), and the *Cxcl8* chemokine mRNA expression in HAECs (Fig. 5A). OA also decreased the ER stress–related transcription factors, namely, *Atf3*, *Atf4*, and *Atf6* mRNA expression (fig. S3 A).

Next, we overexpressed endothelial SCD1 via a recombinant adenovirus-based system to demonstrate a reduced *Cxcl8* and its receptor *Cxcr1* and olfactory receptor 2 (*Or6a2*) mRNA expression (Fig. 5B) (*33*, *34*). Lipidomic analyses revealed that the OA concentration (FA 18:1) was increased in both the intracellular fraction and the conditioned medium following SCD1 overexpression (Fig. 5C). PCA analysis showed that SCD1 overexpression shifted the lipidomic profile compared to the control cells (fig S3, B and C) and increased the MUFA content in triglycerides (fig. S3D). The conditioned medium from HAEC overexpressing SCD1 mitigated LPS-induced inflammatory gene expression in HAECs (Fig. 5D), suggesting that both intracellular and extracellular OA confer anti-inflammatory responses.

Endothelial-specific SCD1 deletion abrogated vascular endothelial protection

To further demonstrate SCD1-mediated vascular protection, we developed endothelial-specific *Scd1* deletion in a $Ldlr^{-/-}$ mouse model of atherosclerosis (*35*, *36*). We generated $Ldlr^{-/-}$ mice with or without endothelial deletion of the *Scd1* gene upon expression of Cre recombinase under the Cdh5 promoter [vascular endothelial cadherin (VE-cadherin)] ($Ldlr^{-/-}$ $Scd1^{EC-/-}$) (*37*). Next, $Ldlr^{-/-}$ or $Ldlr^{-/-}$ $Scd1^{EC-/-}$ mice were fed on HFD for 28 days to develop fatty streaks in the aorta (Fig. 6A). After 14 days, a subset of mice on HFD underwent voluntary wheel running for 14 days (HFD-EX) (refer to fig. S4 and table S2 for body weight gain and exercise duration).

On day 28, targeted quantitative metabolomic analyses revealed that sedentary $Ldlr^{-/-}$ $Scd1^{EC-/-}$ mice developed a trend toward lower basal levels of circulating OA and PA, as compared to the $Ldlr^{-/-}$ mice without SCD1 deletion. Plasma OA and PA levels in the $Ldlr^{-/-}$ $Scd1^{EC-/-}$ mice undergoing exercise remained similar to those of the sedentary group, whereas OA and PA were significantly elevated in the $Ldlr^{-/-}$ mice undergoing exercise (Fig. 6B). Stearic and palmitic acids remained unchanged (fig. S5). These findings support the notion that exercise promotes SCD1-catalyzed plasma OA and PA levels in mice.

As a corollary, in silico simulation revealed that exercise-augmented PSS mitigated flow recirculation along the lesser curvature of the aortic arch (Fig. 7A, top, and fig. S1). Next, en face immunostaining for the ETS-related gene (ERG) nuclear marker for vascular endothelium (*38*) and VCAM1 adhesion molecule were imaged by confocal microscopy. VCAM1 is an early marker of leaky endothelial tight junction in the atheroprone vascular areas (*30*). VCAM1 expression was prominent in the disturbed flow-exposed lesser curvature in $Ldlr^{-/-}$ mice on HFD (top left). SCD1 deletion in $Ldlr^{-/-}$ $Scd1^{EC-/-}$ mice on HFD also developed comparable expression of VCAM1 staining (bottom left). However, voluntary wheel running for 14 days mitigated VCAM1 expression in the $Ldlr^{-/-}$ mice (top right) but not in the $Ldlr^{-/-}$ $Scd1^{EC-/-}$ mice (bottom right) (Fig. 7A; quantification in Fig. 7C).

In the descending aorta where endothelium was exposed to PSS (Fig. 7B, top panels), VCAM1 expression was not observed. Confocal imaging corroborated a low number of VCAM1-positive cells in the descending aorta of HFD-fed $Ldlr^{-/-}$ mice (top left), whereas deletion of endothelial *Scd1* ($Ldlr^{-/-}$ $Scd1^{EC-/-}$) increased the number of VCAM1-positive cells (bottom left). Furthermore, 14-day voluntary exercise did not mitigate VCAM1-positive endothelial cells in $Ldlr^{-/-}$ $Scd1^{EC-/-}$ mice (bottom right) (Fig. 7B, quantification in Fig. 7C).

After exercise, $Ldlr^{-/-}$ mice developed prominent SCD1 staining in the disturbed flow-prone region of the aortic arch, which was absent in $Ldlr^{-/-}$ $Scd1^{EC-/-}$ mice, as evidenced by in situ hybridization with SCD1-specific probe (RNAscope) (Fig. 7E). Thus, exercise-augmented PSS activates endothelial SCD1 to reduce adhesion molecule expression.

Transcriptomic analysis of *Scd1*-positive but *Vcam-1*–negative endothelial subclusters

We performed single-cell RNA sequencing on aortas from $Ldlr^{-/-}$ mice undergoing three conditions: (i) normal chow diet, (ii) HFD, and (iii) HFD-EX for 4 weeks (Fig. 8A). Unbiased clustering analysis of transcriptional profiles identified nine cell types with the specific vascular lineages: B cell, red blood cell, endothelium, fibroblast, macrophage, monocyte, neuron, smooth muscle cell, and T cell (Fig. 8B and fig. S6) plus five endothelial cell subclusters (Fig. 8, C and D).

We identified a defined endothelial subcluster in which higher levels of *Pparγ* and *Scd1* are associated with a low level of *Vcam1* expression (Fig. 8, E and F). Most of the endothelial cells with a higher *Vcam1* expression were associated with HFD. By integrating our endothelial transcriptomic data with a published database (*39*), we used Cytoscape to uncover potential candidate genes interacting with endothelial *Scd1*, including adiponectin receptor 2 (*Adipor2*) (*40*), peroxisomal acyl-CoA oxidase 1 (*Acox1*) (*41*, *42*), and insulin receptor substrate 2 (*Irs2*) (fig. S7) (*43*–*45*).

DISCUSSION

Cardiometabolic diseases predispose individuals to develop acute coronary syndromes and stroke, thus increasing health care burden (*46*). While exercise is an effective lifestyle modification to ameliorate cardiometabolic disease, elucidating the flow-sensitive metabolic transducers has the potential to identify therapeutic targets for individuals who are unable to engage in physical activities. In this study, we demonstrate that wheel running exercise activates endothelial SCD1 to catalyze vascular protective lipid metabolites. By integrating the dynamic flow system, metabolomic analyses, Doppler ultrasound to reconstruct fluid-structure interface for in silico analysis, and a voluntary wheel running system, we demonstrated that exercise augments PSS to activate endothelial SCD1 in the disturbed flow-prone aortic arch (Fig. 9 and fig. S8). Deletion or overexpression of endothelial-specific SCD1 demonstrated that exercise-activated SCD1 catalyzes the lipid metabolite, OA, to attenuate both inflammatory and atherosclerotic mediators.

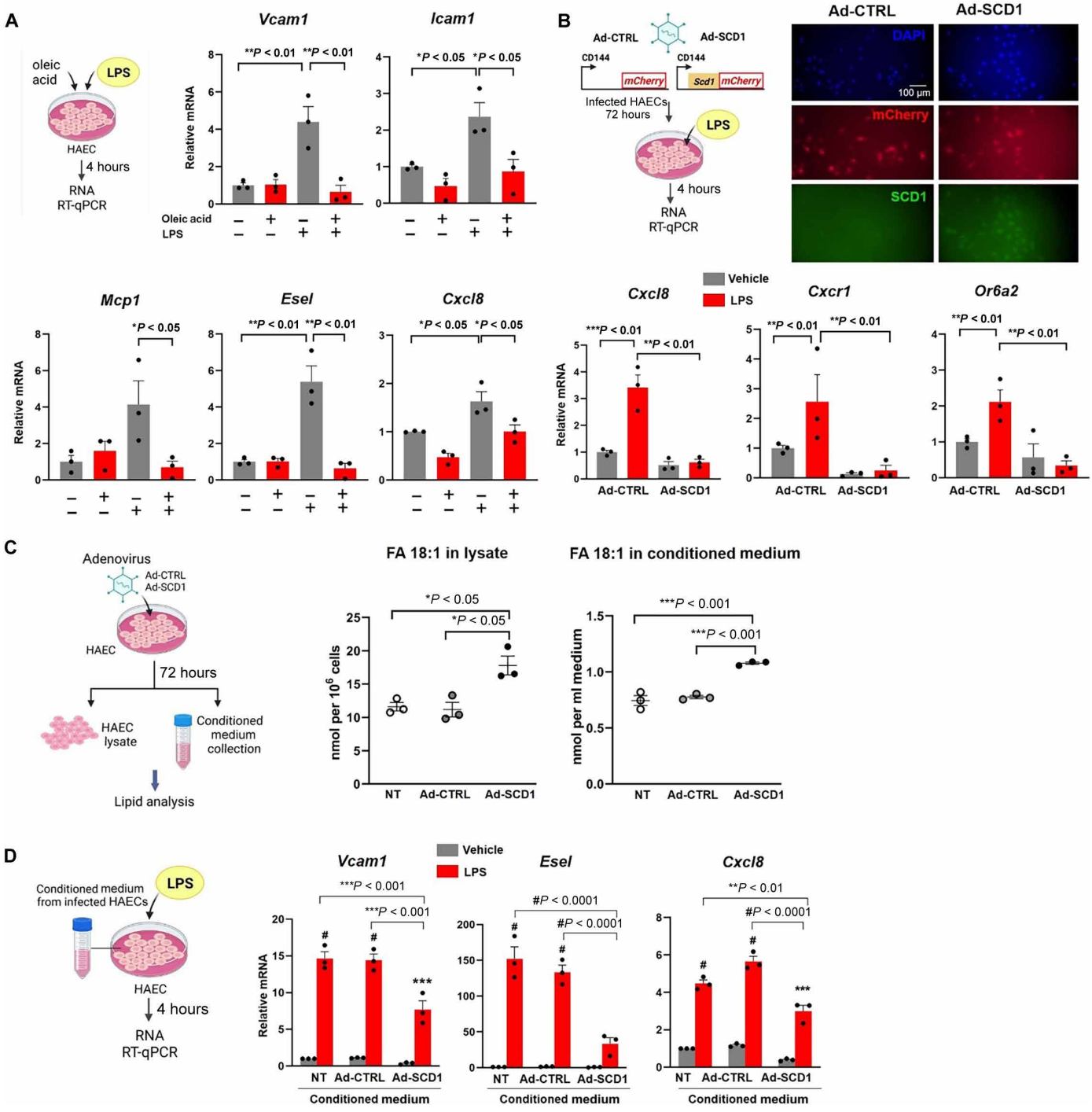

Fig. 5. OA treatment or SCD1 overexpression mitigate pro-inflammatory mediators in HAEC. (**A**) HAEC monolayers were treated for 4 hours with OA at 0.2 mM in the absence or presence of lipopolysaccharide (LPS; 20 ng/ml) and reverse transcription quantitative polymerase chain reaction (RT-qPCR) was performed. (**B**) HAECs were infected with adenovirus control or adenovirus to overexpress SCD1 and subjected to LPS treatment. Transfection was validated using immunostaining for mCherry reporter and SCD1 expression. Ad-SCD1 mitigated the LPS -induced expression (4 hours) of *Cxcl8*, *Cxcr1*, and *Or6a2* (*$P < 0.05$, **$P < 0.01$, and ***$P < 0.001$; $n = 3$). DAPI, 4′,6-diamidino-2-phenylindole. (**C**) HAECs were transfected with adenovirus control or adenovirus to overexpress SCD1. After 72 hours, the conditioned medium, and the cellular lysate were collected and processed for lipidomic analysis. The fatty acid (18:1) content corresponding to OA was normalized to the number of cells in the lysate or the volume of conditioned medium [*$P < 0.05$, **$P < 0.01$, and ***$P < 0.001$; $n = 3$, one-way analysis of variance (ANOVA)]. Non-transfected cells (NT) were also included as control. (**D**) HAEC monolayers grown in regular culture medium were changed to conditioned medium collected from HAECs from NT, Ad-CTRL, and Ad-SCD1 in the presence or absence of LPS (20 ng/ml) for 4 hours). RT-qPCR for inflammatory gene expression was performed medium (**$P < 0.01$, ***$P < 0.001$, and #$P < 0.0001$; $n = 3$, two-way ANOVA).

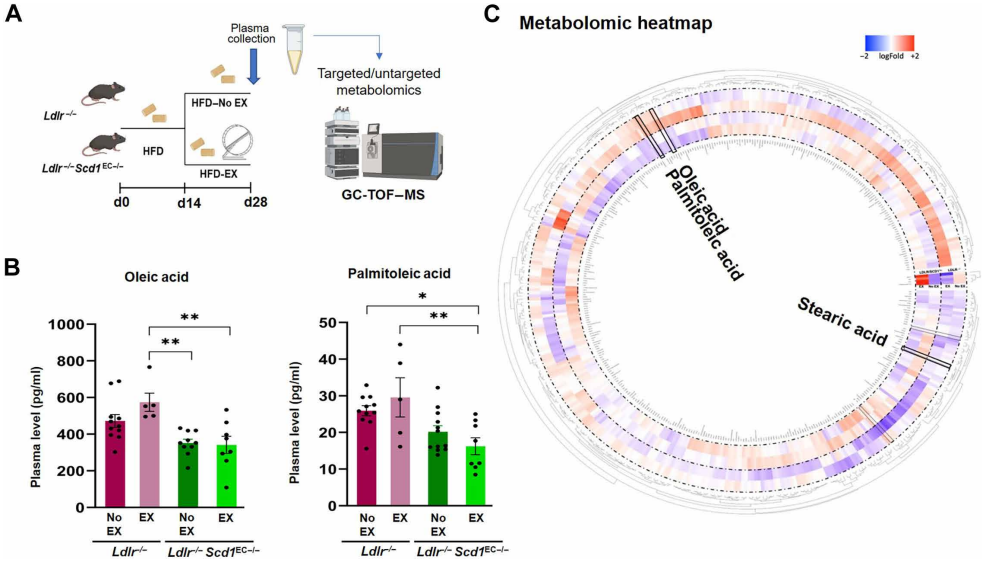

Fig. 6. Exercise-mediated lipid metabolites OA and PA are reduced in mice with endothelial-specific *Scd1* deletion. (**A**) The experimental protocol depicts the *Ldlr*$^{-/-}$ mice that were crossed with *Cdh5Cre*; *Scd1*$^{flox/flox}$ to generate endothelial-specific SCD1 deletion (*Ldlr*$^{-/-}$ *Scd1*$^{EC-/-}$). Adult mice at 8 weeks were fed HFD for 14 days. The HFD-fed mice were then divided into exercise (EX) and no exercise (No EX) arms for additional 14 days while continuing HFD. GC-TOF-MS, gas chromatography time-of-flight mass spectrometry. (**B**) The absolute plasma OA concentration was elevated after exercise in the *Ldlr*$^{-/-}$ mice, whereas OA concentration was reduced and remained reduced after exercise in the *Ldlr*$^{-/-}$ *Scd1*$^{EC-/-}$ mice. The plasma concentration of PA also followed a similar trend, suggesting that exercise activates SCD1 to catalyze OA and PA (*$P < 0.05$ and **$P < 0.01$; $n = 4$ to 12; two-way ANOVA; each dot represents an individual animal). (**C**) Circular heatmap of untargeted metabolomic analysis captures the known and unknown identity (ID) metabolites and highlights changes in OA and PA after normalization and scaling using the Pareto method. The circular heatmap further supports that *Scd1* deletion resulted in a decrease in both OA and PA. Circular heatmap was generated with Circos R package.

Hemodynamic shear stress modulates vascular metabolism to maintain endothelial homeostasis (*47*, *48*), and PSS is atheroprotective, attenuating the proinflammatory mediators and NADPH oxidase system (*4*, *6*, *25*, *49*). Our metabolomic analysis revealed that PSS increased SCD1-catalyzed fatty acid metabolites, and this observation led to the investigation of exercise-activated SCD1 as a metabolomic transducer to mitigate both inflammatory mediators and ER stress.

SCD1 is highly expressed in multiorgan systems as an enzyme anchored in the ER to catalyze saturated FAs, including palmitic (16:0) and stearic (18:0). The resulting MUFAs, PA (16:1) and OA (18:1), are the major components of triglycerides, cholesterol esters, and phospholipids (*23*, *50*). Using subcellular fractioning, previous studies indicated that SCD1 is localized in the MAM, a specific region of the ER in proximity to the outer mitochondrial membrane that is enriched in enzymes responsible for phospholipid and triglyceride biosynthesis (*22*). SCD1 is expressed at high levels in the insulin-sensitive hepatocytes and white and brown adipocytes (*51*, *52*). Other tissue-specific SCD isoforms have also been identified, including SCD2 in the brain (*53*), SCD3 in the skin and sebaceous gland (*54*), and SCD4 in the heart (*55*). Vascular endothelial SCD1 has not been well investigated, mainly due to the relatively lower basal expression compared to other organs, such as the liver, adipose tissue, and skeletal muscle (*51*, *52*, *56*). In addition, there are experimental challenges to accurately assess metabolomic profiles in isolated endothelial cells. In our study, we first identified SCD1-catalyzed metabolites in HAEC lysates following OSS or PSS conditions. To validate these metabolites in vivo, we collected plasma metabolomic data from mice following wheel running exercise for 24 hours. While plasma metabolomics may also reflect metabolite contributions from other organs, we were able to demonstrate reduced levels of OA and PA in the endothelial SCD1–deleted mice (*Scd1*$^{EC-/-}$) undergoing exercise. SCD1 leads to desaturation of SFAs to facilitate their esterification and storage, thereby preventing downstream lipotoxicity in HAECs (*57*). Our lipidomic analyses suggest that PSS-mediated activation of endothelial SCD1 promotes both intracellular and circulating pools of OA to confer endothelial protection.

The expression of SCD isoforms is highly regulated by multiple factors, including diets and hormones (*58*). SCD1 expression is associated with adipose, cancer cell, and skeletal muscle metabolism, and hepatic and pulmonary fibrosis (*59*–*61*). Global deficiency in SCD1 results in reduced adiposity, increased insulin sensitivity, and resistance to diet-induced obesity (*62*). The global deletion of SCD1 in *Ldlr* null background leads to abnormal lipid metabolism, ER stress, inflammation, and atherosclerosis (*63*). Furthermore, the strength of hand grip, swimming duration to exhaustion, and voluntary versus forced treadmill wheel running support that SCD1 overexpression increases cardiovascular endurance (*64*). SCD1-derived lipokine prevents cytotoxic stress by inhibiting p38 mitogen-activated protein kinase activation; contracts unfolded protein response (UPR), ER-associated protein degradation, and apoptosis; regulates autophagy; and maintains cell morphology and proliferation (*65*). However, SCD1 also impairs the reparative properties of macrophages and microglia in the brain (*66*). SCD1 can act as an autophagy inducer or inhibitor in cancer depending upon the degree of cancer heterogeneity and plasticity (*67*). Nevertheless, these studies all identify SCD1 as a therapeutic target for metabolic disorders.

In this context, we developed the endothelial-specific *Scd1* deletion in *Ldlr*$^{-/-}$ mice. During exercise, autonomic function elevates

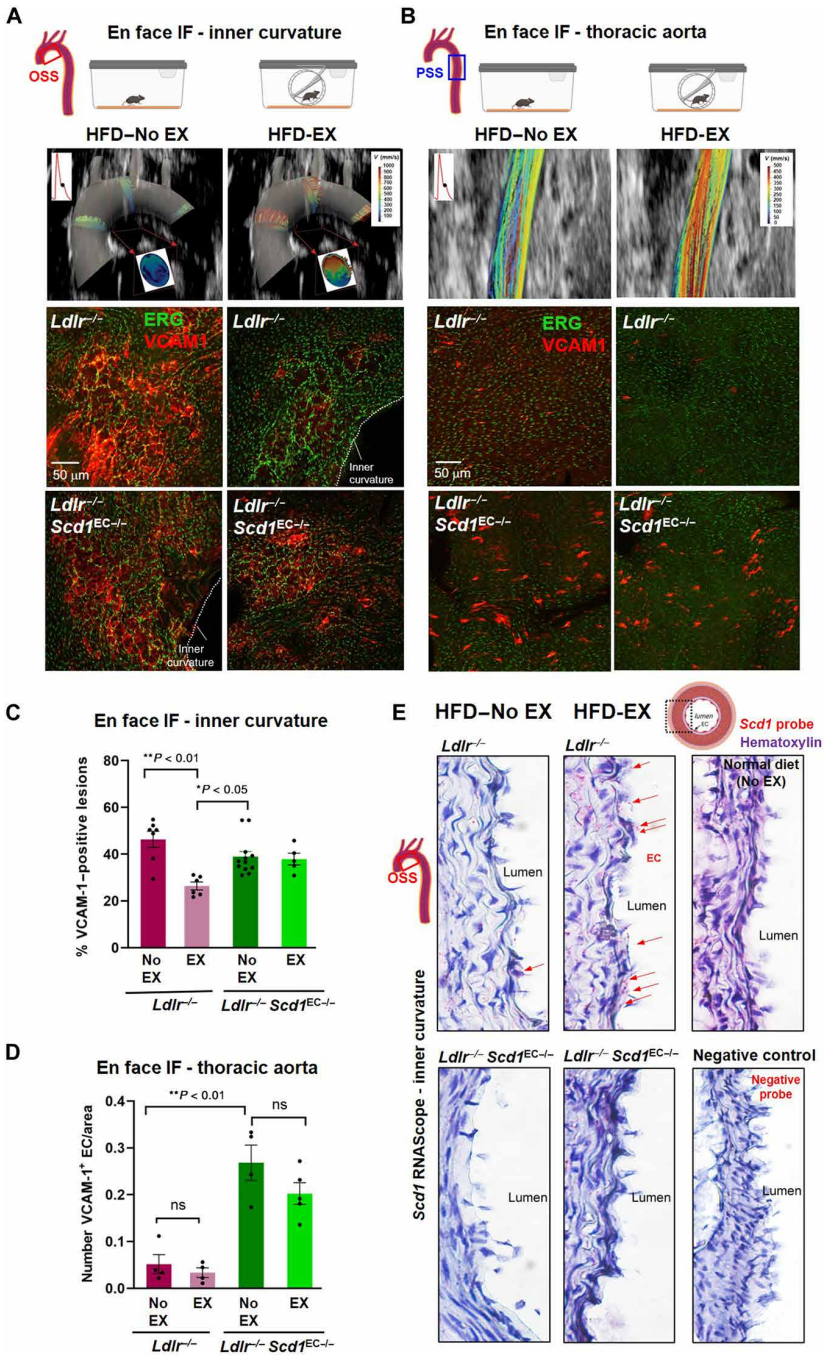

Fig. 7. Endothelial-specific *Scd1* deletion abrogates exercise-mediated anti-inflammatory mediators. The experimental design is described in Fig. 6A. (**A** and **B**) Top panels: CFD simulates the spatial and temporal variations in WSS in the aortic arch versus descending aorta. The ultrasound B-mode was used to reconstruct the 4D shear stress profiles. The cross sections of the aortic arch illustrate the high shear stress along the greater curvature but low shear stress along the lesser curvature. Exercise mitigates disturbed flow at the lesser curvature. The CFD reconstruction over a cardiac a cardiac cycle (t_1, t_2, and t_3) is included in fig. S3; only t_2 is depicted here. The colored streamlines indicate the CFD-derived velocity profiles along the aortic arch. Representative confocal *Z*-stacks for the maximal projection of en face immunostaining with anti-ERG and anti-VCAM1 in the inner curvature versus the thoracic region of the descending aorta. In the lesser curvature, the VCAM1 staining was attenuated following exercise in the *Ldlr*$^{-/-}$ mice but remained in the *Ldlr*$^{-/-}$ *Scd1*$^{EC-/-}$ mice. In the thoracic aorta, VCAM1 staining was reduced with or without exercise in the *Ldlr*$^{-/-}$ mice but was elevated with or without exercise in the *Ldlr*$^{-/-}$ *Scd1*$^{EC-/-}$ mice. This finding supports that PSS activates endothelial SCD1 to mitigate arterial inflammation. (**C** and **D**) Quantification of en face immunostaining shown in (A) and (B), respectively. Each dot corresponds to an individual animal ($n = 4$ to 12); both male and female data were pooled together. ns, not significant; IF, immunofluorescence. (**E**) SCD1-specific probe (RNAscope) corroborates prominent endothelial SCD1 staining following exercise in the disturbed flow-prone aortic arch in *Ldlr*$^{-/-}$ mice but not in *Ldlr*$^{-/-}$ *Scd1*$^{EC-/-}$ mice. *Scd1* expression remains unchanged after HFD as compared to normal chow diet. Red dots (arrows) indicate mRNA molecules in the intima layer. Staining with a negative control probe (bottom right) shows complete absence of red dots. Microphotographs were taken at ×63.

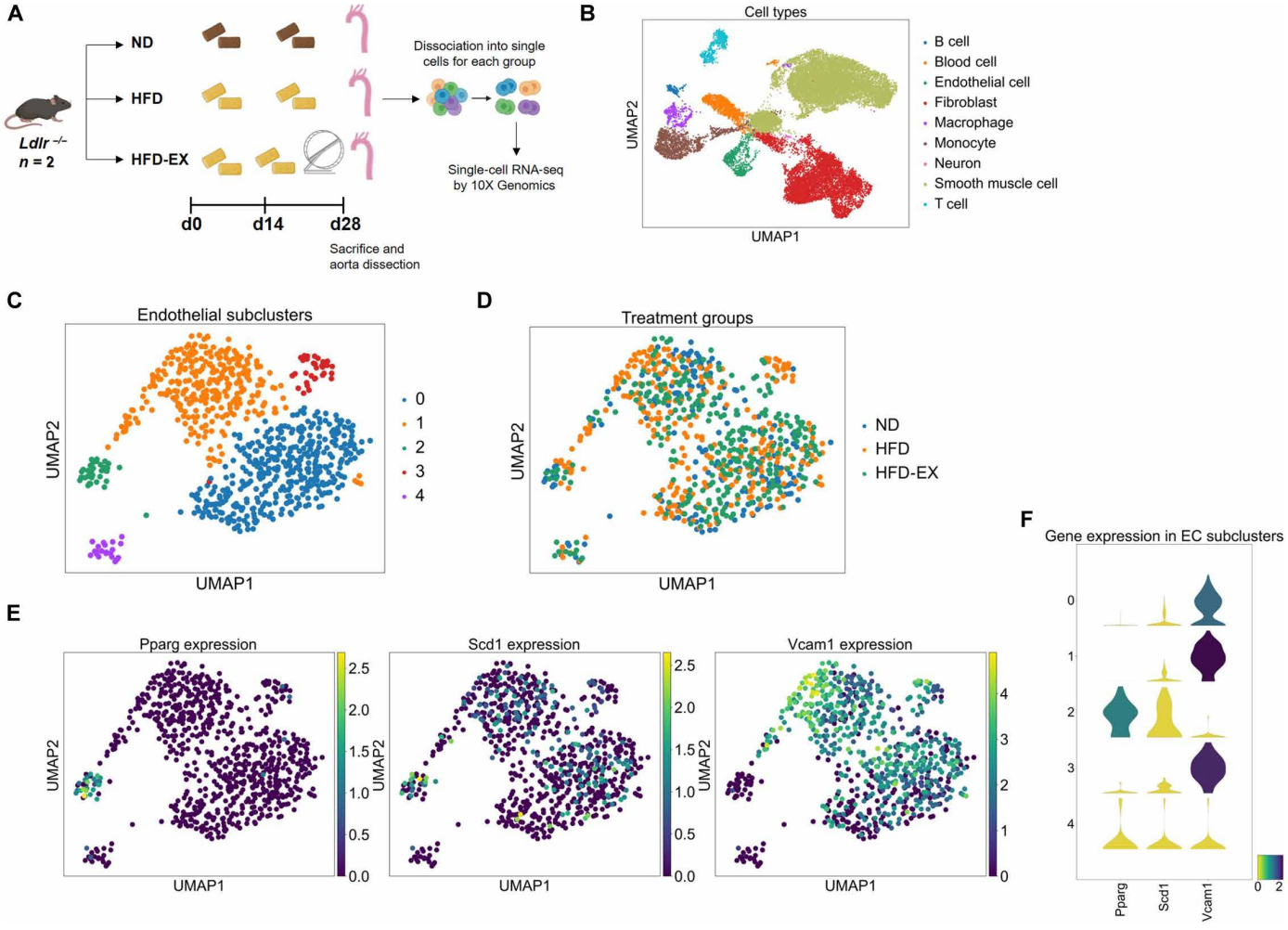

Fig. 8. Single-cell transcriptomic analysis of the mouse aorta. (**A**) Schematic diagram of the experimental protocol. *Ldlr*$^{-/-}$ mice ($n = 2$ per group) were subjected to normal chow diet (ND, control), HFD, or HFD plus 2-week exercise (HFD-EX). Aortas were collected after 28 days. A total of 20,000 cells were analyzed. (**B**) Representative uniform manifold approximation and projection (UMAP) of cellular clusters in the mouse aorta indicates nine cell types with specific vascular lineages. (**C** and **D**) Representative UMAP of endothelial cells in the mouse aorta indicates the presence of five subclusters across the three experimental conditions. (**E** and **F**) Changes in *Pparγ*, *Scd1*, and *Vcam1* expression identify an endothelial subcluster in which higher levels of *Pparγ* and *Scd1* are associated with a low level of *Vcam1* expression.

both BP and HR, thus leading to increased blood flow and shear stress (*68*). By deploying the micro shear stress sensors into the rabbit aorta, we previously demonstrated a positive correlation between BP/HR and PSS (*69*). For this reason, the wild-type mice undergoing 2 weeks of wheel running developed PSS-activated endothelial SCD1 expression, as evidenced by in situ hybridization and en face immunostaining of the aortas. This observation supports that exercise-augmented PSS activates endothelial SCD1 expression.

The salutary effects of exercise are well recognized to maintain endothelial homeostasis and to mitigate oxidative stress and inflammatory response (*70*). Exercise elevates the serum clusterin that increases plasticity and reduces inflammation in the cerebrovascular system (*14*). Recently, exercise was reported to increase both the human and racehorse plasma metabolite, *N*-lactoyl-phenylalanine (Lac-Phe), which suppressed feeding and obesity in mice (*71*). However, individuals with physical disabilities may have reduced capacity to perform regular exercise. In addition, sedentary lifestyle remains prevalent in the industrialized nations. For this reason, the National Institutes of Health (NIH) Molecular Transducers of Physical Activity Consortium was established to integrate large-scale multi-omics analyses with bioinformatics to identify molecular transducers to mimic the therapeutic effects of exercise (*15*). Several signaling pathways have been identified, including insulin-like growth factor 1/phosphatidylinositol 3-kinase/Akt, CCAAT/enhancer binding protein/CITED4, PPAR family, PGC1α, AMPK, eNOS/NO, and, recently, noncoding RNAs (*72*).

PPARs belong to the nuclear receptor superfamily of ligand-activated transcription factors regulating lipid and glucose metabolism, energy homeostasis, and inflammation (*73*). Previous studies have demonstrated that shear stress induces PPARα, PPARδ, and PPARγ to regulate endothelial function (*74*, *75*). PPARγ agonists belong to the thiazolidinedione class of drugs such as troglitazone and rosiglitazone that attenuate palmitate-induced ER stress and apoptosis by activating SCD1 induction in macrophages (*76*). PPARγ was shown to protect against interleukin-1β (IL-1β)–mediated endothelial

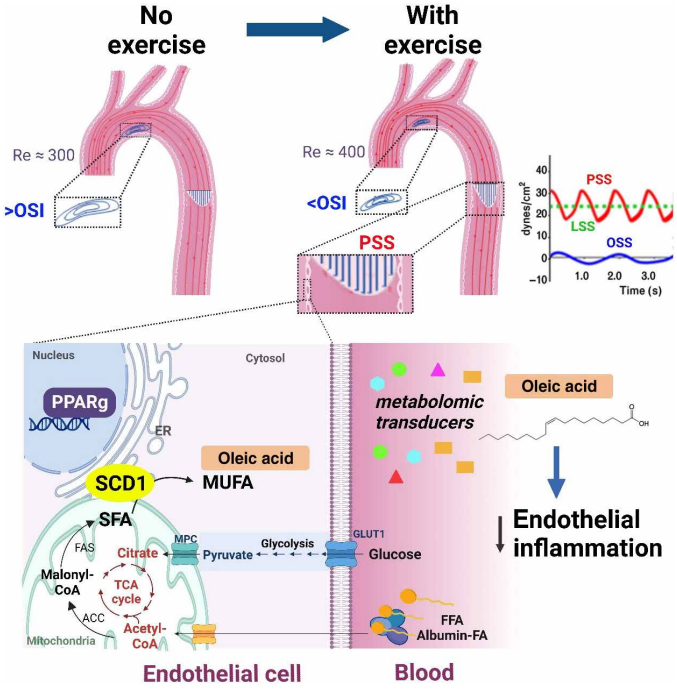

Fig. 9. Schematic model for exercise-augmented PSS in the aorta and activation of the flow-responsive PPARγ-SCD1 pathway for atheroprotective metabolites. Exercise-mitigates flow recirculation and OSI in the aortic arch. SCD1 located in the ER membrane catalyzes SFA to MUFA, leading to increased intracellular and circulating levels of OA. OA inhibits NF-κB–mediated inflammation markers in the endothelium. MPC, mitochondrial pyruvate carrier; TCA, tricarboxylic acid; ACC, acetyl-CoA carboxylase; FAS, fatty acid synthase.

dysfunction through a reduction in oxidative stress (*77*) and mitigate aging-associated endothelial dysfunction (*78*). For these reasons, small interfering RNA silencing of endothelial PPARγ (fig. S9, A to C) versus treating HAECS with PPARγ-agonist rosiglitazone (fig. S9D) revealed that PSS-activated endothelial SCD1 expression is PPARγ-dependent, as previously reported (*24*). In addition, transgenic mice expressing a dominant-negative V290M PPARγ mutation in endothelial cells (E-V290M Tg) (*79*) developed a reduction in endothelial SCD1 expression in the aorta in response to exercise (fig. S10).

It is well recognized that mice with mutation in the low-density lipoprotein receptor ($Ldlr^{-/-}$) develop atherosclerotic lesions upon HFD feeding (*35*, *36*). These atherosclerotic lesions preferentially develop at the disturbed flow-exposed arterial bifurcation or the aortic inner curvature (*80*). Disturbed flow or OSS increased VCAM1 expression, Ly6G-positive neutrophil recruitment, and subsequent accumulation of erythrocyte-derived iron and lipid droplets to initiate the atherosclerotic lesions known as fatty streaks (*30*). In our study, VCAM1 expression was prominent in the lesser curvature of the aorta in HFD-fed $Ldlr^{-/-}$ mice but absent in the PSS-exposed descending aorta. After 14 days of exercise, the VCAM1 positive lesions were attenuated in the lesser curvature in $Ldlr^{-/-}$ but not $Ldlr^{-/-}$ $Scd1^{EC-/-}$ mice, supporting the notion that exercise-activated SCD1 mitigates inflammatory mediators. Furthermore, *Scd1* deletion in $Ldlr^{-/-}$ mice promoted endothelial inflammation, including the PSS-exposed descending aorta (Fig. 7). Furthermore, exercise did not mitigate the number of VCAM1-positive cells in $Scd1^{EC-/-}$, supporting exercise-activated SCD1 for vascular protection.

Diets enriched in SFAs are linked to increased cardiovascular disease risk, whereas MUFAs have been associated with improved cardiovascular outcomes (*81*). OA is the predominant MUFA in the Mediterranean diets, including olive oil as the principal source of fat. Our in vitro results are consistent with the previous reports that OA inhibits LPS-induced endothelial oxidation (*82*–*84*), reduces NF-κB activation (*85*), and ameliorates insulin resistance (*83*). In our study, both OA treatment or SCD1 overexpression reduced the endothelial expression of *Cxcl8* (IL-8), which is a member of the proinflammatory chemokine family through CXCR1 and CXCR2 receptors (*33*). In this context, SCD1 deficiency predisposes to cellular ER stress, which activates the UPR by increasing activating transcription factor 6 (ATF6) production, and ER stress–mediated signaling pathways (*86*–*88*), whereas SCD1 overexpression reduced the *Or6a2* expression as the murine ortholog *Olfr2* in macrophages to promote atherosclerosis (*34*).

In parallel, our network analysis of endothelial transcriptomic profiles in response to HFD versus exercise-induced PSS uncovered three candidate genes interacting with *Scd1* that deserve further investigation: *Adipor2* regulates the membrane fluidity by maintaining MUFA levels in HEK293 cells (*89*), *Acox1* protects against LPS-driven inflammation (*41*), and *Irs2* regulates eNOS phosphorylation and glucose uptake by skeletal muscle (*43*–*45*).

In summary, exercise-augmented PSS activates endothelial SCD1 to catalyze vascular protective lipid metabolites, OA and PA. While SCD1 is associated with cross-tissue metabolism, we reveal endothelial-specific SCD1 to mitigate inflammatory responses in the disturbed flow-exposed aortic arch. Overall, integration of genetic mouse models, voluntary exercise, and in silico analysis provides insights into the flow-responsive SCD1 as a metabolic transducer to mitigate cardiometabolic disorders.

Limitations of the study

Our study focuses on the initiation of atherosclerosis in the disturbed flow-exposed aorta in HFD-fed $Ldlr^{-/-}$ mice followed by a short period of exercise (2 weeks). Voluntary wheel running method was adopted for exercise training to simulate the nocturnal running behavior. Other approaches, including forced recurrent treadmill running and forced swimming, require a stimulus (such as an electric shock) in association with stress to the animals.

MATERIALS AND METHODS

Mice lines

Male and female C57BL/6J mice from the Jackson Laboratory (strain 000664) were used for the exercise studies. The endothelial dominant-negative *Pparγ* (EC-DN-*Pparγ*) mice line was provided by C. D. Sigmund at the University of Iowa. These mice express a human dominant negative *Pparγ* variant with the human V290 mutation under the control of the endothelial-specific *Cdh5* promoter (*79*).

Mice carrying the $Ldlr^{tm1Her}$ mutation were obtained from the Jackson Laboratory (strain 002207) to generate $Ldlr^{tm1Her/tm1Her}$ ($Ldlr^{-/-}$) mice. To study SCD1-mediated arterial inflammation, $Ldlr^{-/-}$ were crossed with mice carrying a conditional mutation of the *Scd1* gene ($Scd1^{flox/flox}$) generated by James Ntambi lab at the University of Wisconsin Madison (*51*, *90*). The endothelial deletion of *Scd1* gene was achieved by Cre recombination with $Cdh5Cre^{+}$ mice, in which the *Cdh5* promoter (also known as *VE-Cadherin*) drives the

constitutive expression of *Cre* in endothelial cells. *Cdh5Cre* mice were obtained from the laboratory of L. Iruela-Arispe (*37*). $Ldlr^{-/-}$, $Scd1^{flox/flox}$, $Cdh5^{Cre}$ mice (subsequently called $Ldlr^{-/-}$ $Scd1^{EC-/-}$) were generated through appropriate breeding schemes and polymerase chain reaction (PCR) genotyping in tail DNA. Littermates $Ldlr^{-/-}$, $Scd1^{flox/flox}$ (or $Ldlr^{-/-}$ for simplicity) were used as controls. All mice were maintained on a C57BL/6J genetic background to reduce genetic variability.

Ldlr null mice to develop fatty streaks

$Ldlr^{-/-}$ and $Ldlr^{-/-}$ $Scd1^{EC-/-}$ mice at 6 to 8 weeks of age were used for all our studies. Mice were fed a HFD (Teklad, TD.88137, Envigo, Indianapolis, IN, USA) for 4 weeks. The formulation is highly enriched in SFAs (>60% of total fatty acids) and contains 42% kcal from fat. The diet was supplied as soft pellets and replaced every 2 to 3 days to ensure freshness. After 2 weeks, randomly selected animals from each genotype group were transferred to individual exercise cages and continued receiving HFD for 2 more weeks (Fig. 5A).

Voluntary wheel exercise studies

The wild-type C57BL/6J mice fed a regular rodent chow or the $Ldlr^{-/-}$ and $Ldlr^{-/-}$ $Scd1^{EC-/-}$ mice on HFD were assigned to exercise. They were transferred to individual polycarbonate cages with a stainless-steel running wheel. Each wheel had an automated counter to record the distance and speed at which each animal ran in either direction (BIO-ACTIVW-SOFT from Bioseb, Pinellas Park, FL, USA). Spontaneous wheel running was monitored continuously over 2 weeks. Animals received food and water ad libitum during the data collection period. Mice in the no exercise group were housed in regular static cages in the same testing room to minimize environmental variations.

For studies with 24 hours of voluntary exercise, blood samples were collected from the retroorbital plexus of 8-week-old male wild-type C57BL/6J mice at baseline between 8:00 and 9:00 a.m. The mice were immediately transferred to the exercise cages for overnight running. Next morning, blood was collected between 8:00 and 9:00 a.m. Plasmas were separated and processed as described in Supplementary Methods.

Quantification of arterial shear strain and wall shear stress after exercise

We used the B-mode images of the aortic arch to simulate the time-dependent 3D CFD model, and we reconstructed a 3D model of the lumen structure by resolving the vessel wall curvature along the centerline of the aorta and its branches (MATLAB). To obtain the boundary conditions for our in silico analysis of exercise-augmented PSS, we interrogated the mouse aortic arch via an ultrasound transducer (Vevo 3100, FUJIFILM VisualSonics) (Fig. 2A and C). ECG-gated PW Doppler was acquired for the inlet boundary condition of the time-dependent flow of the aortic arch. This inlet condition was calibrated for the exercise model as previously reported (*27*, *28*). For the boundary condition at the four outlets of the model, namely, brachiocephalic, left common carotid, left subclavian artery, and descending aorta, from the three-element Windkessel model (*29*).

TAWSS ($\mathrm{TAWSS} = \frac{1}{T}\int_0^T |\mathrm{WSS}|\,dt$) contours, OSI $\left[\mathrm{OSI} = \frac{1}{2}\left(1 - \frac{\left|\int_0^T \mathrm{WSS}\ dt\right|}{\int_0^T |\mathrm{WSS}|dt}\right)\right]$, and velocity profiles for a time-dependent model were acquired by solving the Navier-Stokes equations using the using svFSI solver (*91*)

$$\rho\left(\frac{\partial \vec{V}}{\partial t} + \vec{V}\,.\,\nabla\vec{V}\right) = -\nabla P + \mu\nabla^2\vec{V}$$

$$\nabla\,.\,\vec{V} = 0$$

A dynamic flow system to simulate PSS profiles

A dynamic flow channel was used to recapitulate hemodynamics of human carotid arterial bifurcations (*25*, *92*). The flow system was designed to generate well-defined flow profiles across the width of the parallel flow chamber at various temporal gradients ($\partial\tau/\partial t$), frequencies, and amplitudes. ECs were maintained in Dulbecco's modified Eagle's medium culture (DMEM) supplemented with 1% fetal bovine serum at 37°C and pH 7.4 during flow exposure.

Metabolite samples were collected from confluent HAEC monolayers exposed to PSS ($\tau_{ave} = 50$ dyne cm^{-2} accompanied by $\partial\tau/\partial t = 71$ dyne cm^{-2} s^{-1} at 1 Hz), OSS (0.1 to 4 dyne cm^{-2}), or static conditions for 4 hours. Cells were trypsinized and fixed in 4% paraformaldehyde (PFA), and the lysates were immediately stored at −80°C until submission for metabolomic analysis.

Metabolomic analysis

The metabolomic analyses in mouse plasma samples or endothelial cell lysates were performed at the West Coast Metabolomics Center at the University of California Davis, CA. Gas chromatography time-of-flight mass spectrometry untargeted analysis identified 170 known metabolites and 290 unknown compounds. Metabolites were reported with retention index, quantification mass, and full mass spectra. Relative quantification was assessed by peak height. Targeted assays for selected fatty acid metabolites were performed for absolute quantification using stable isotope-labeled internal standards.

The data analysis was performed using MetaboAnalyst 5.0 (Research Resource Identifier RRID:SCR_015539). Before performing PCA, the concentrations of subjected metabolites were corrected using the Pareto scaling method to normalize the measurements of different metabolites on the close scale. The *x* axis in the figures was depicted as the first principal component (PC1) representing the space with the largest variance in data, whereas the *y* axis was depicted as the second principal component (PC2) representing the space with the second largest variance. The ovals are 95% inertia ellipses. Our heatmaps were created using the heatmap.2 program in the "gplots" package of R (http://cran.r-project.org). Circlize package R was used to generate circular heatmap and hierarchical clustering. DESeq was used for normalization. All heatmaps shown are row-normalized for presentation purposes.

SCD1 overexpression via adenovirus

The replication-defective adenovirus Ad5/F35 was designed using the licensed VectorBuilder software. The vector pAd5/F35[Exp]-mCherry-Cd144>mSCD1 (NM_009127.4) contains the Cdh5 promoter to confer endothelial specificity, mCherry as a reporter to allow for visualization of targeted ECs, and the sequence of mouse *Sdc1* (NM_009127.4). The adenovirus was generated by standard laboratory procedures in biosafety level 2 (BSL2) biosafety cabinets using 293A cells. On the day of transfection, recombinant adenoviral plasmids were digested by the restriction enzyme Pac I. The cells were transfected with Lipofectamine-DNA mix (Thermo Fisher Scientific) according to the manufacturer's instructions. Lipofectamine-DNA mix was added to the culture flasks, which were returned to

CO_2 incubator at 37°C. The virus was left to infect the 293A cells and then purified through a centrifugation process. Control adenovirus was (pAd5/F35[Exp]-mCherry-Cd144). The adenovirus title was determined using a standard cytopathic effect assay (CPE) using serial viral dilutions.

HAECs were seeded in T75 flasks and infected the next day with multiplicity of infection (MOI) of 350 of Ad-CTRL or Ad-SCD1, and the medium was replaced with 12 ml of fresh medium. Flasks without adenovirus infection were included as controls. After 72 hours, the conditioned medium was collected, centrifuged 5 min at 1000 rpm to eliminate debris and immediately frozen at −80°C for lipidomic analysis. HAECs were trypsinized and resuspended in phosphate-buffered saline (PBS). Following cell number count, the cellular fraction was stored at −80°C for lipidomic analysis.

Lipidomic analysis

Lipidomic analysis was performed at the University of California Los Angeles (UCLA) Lipidomic Core. A modified Bligh and Dyer extraction (*93*) was carried out on HAEC lysates or conditioned medium aliquots. Before biphasic extraction, a standard mixture of 75 lipid standards (Avanti, 330820, 861809, 330729, 330727, and 791642) was added to each sample. Following two successive extractions, pooled organic layers were dried down in a Thermo SpeedVac SPD300DDA using ramp setting 4 at 35°C for 45 min with a total run time of 90 min. Lipid samples were resuspended in 1:1 methanol:dichloromethane with 10 mM ammonium acetate and transferred to robovials (Thermo Fisher Scientific, 10800107) for analysis.

Samples were analyzed by direct infusion on a Sciex 5500 with Differential Mobility Device (DMS) (comparable to Sciex Lipidyzer platform) with a targeted acquisition list consisting of 1450 lipid species across 17 subclasses. The DMS was tuned with EquiSPLASH LIPIDOMIX (Avanti, 330731). Data analysis was performed with in-house data analysis workflow. Instrument settings, multiple reaction monitoring (MRM) lists, and analysis method are previously described (*94*). Quantitative values were normalized to cell counts or medium volume.

Conditioned medium experiments

HAECs were seeded in regular endothelial cell culture medium. Next day, the medium was replaced with conditioned medium obtained from HAECs under non-transfected, Ad-CTRL, or Ad-SCD1 conditions, without or with LPS at 20 ng/ml (Sigma-Aldrich) for 4 hours. RNA was extracted and inflammatory gene expression was evaluated by reverse transcription quantitative PCR (RT-qPCR).

En face immunostaining of whole-mounted aortas

Thoracic aortas were dissected under a stereomicroscope to remove the perivascular adventitial fat, thus allowing for visualization of the carotid, innominate, and subclavian branches of the aortic arch (*95*, *96*). The aortas were cut longitudinally and pinned on petri dishes filled with a 3-mm coating of polydimethylsiloxane (Sylgard 184 Elastomer Kit, Dow Corning Corporation) using minutien pins of 0.1-mm diameter (Fine Science Tools). Aortas were fixed in the open flat conformation for 2 to 4 additional hours in 4% PFA and washed with PBS. After permeabilization and blocking with 3% goat serum (Thermo Fisher Scientific, catalog no. 50062Z) containing 0.3% Triton X-100 and 0.1% Tween 20, aortas were incubated in 12-well dishes with anti-ERG rabbit monoclonal antibody (1:200; Abcam, no. ab92513), anti-VCAM1 rat monoclonal antibody (1:100; BD Biosciences, no. 550547), or anti-SCD1 rabbit antibody (1:100; Cell Signaling Technology, no. 2794). Fluorescently labeled secondary antibodies (Life Science Technologies) were applied at 1:250 dilution. Nuclei were counterstained with Hoechst 33258 (Thermo Fisher Scientific, no. H1398). The aortas were mounted with the endothelial layer facing up on microscopic slides using ProLong Gold antifade mounting medium (Thermo Fisher Scientific) and covered with a glass coverslip under light pressure to flatten the preparation. The images of the inner curvature and descending aorta were captured with 10×, 20×, or 63× objective on a Zeiss LSM710 or LSM900 confocal microscope with ZEN acquisition software (Carl Zeiss Microscopy). The endothelial layer of the whole mount preparation was identified by positive ERG endothelial nuclear marker staining and the morphological features of the nuclei. Image processing of maximal projections of the *Z*-stacks and blind quantification were performed with NIH Fiji software.

Single-cell RNA sequencing

The complete aorta was perfused with cold PBS, isolated, and dissected to eliminate the surrounding periaortic fat. After mincing with scissors, a single-cell suspension was obtained through enzymatic digestion with elastase (Worthington, Lakewood, NJ, USA) and liberase (Roche, Basel, Switzerland) at 37°C. The preparation was passed through a 70-μm filter and treated with a Red Blood Cell lysis buffer (Abcam, Waltham, MA, USA). Single cells were resuspended in PBS containing 0.04% bovine serum albumin, counted, and assessed for viability using Trypan Blue.

Single-cell RNA sequencing was performed using the 10X Genomics Chromium platform at the UCLA Technology Center for Genomics and Bioinformatics. Raw sequencing data were demultiplexed and aligned using the Cell Ranger software from 10X Genomics, and the gene expression count matrix from Cell Ranger was obtained for downstream analyses.

Single-cell RNA data analysis

The raw fastq scRNA reads were processed using Cell Ranger software (10X Genomics) and subjected to quality control with FastQC. The resulting output data for the three treatment groups were analyzed with the Scanpy package in Python. To generate an annotated data object, the data from the treatment groups were concatenated. Cells with gene counts above 4000 or below 200 were filtered, as were those with a mitochondrial gene count exceeding 10%. Subsequently, we performed normalization, PCA, variable gene extraction, nonlinear dimensional reduction, and clustering to produce uniform manifold approximation and projection plots and identify cell clusters using marker genes. To visualize gene expressions between categories of related diet ± exercise, we created a circular heatmap. Circular heatmap features the $\log_2$ transformation of the fold changes, calculated as described above. Our heatmaps were created using the heatmap.2 program in the "gplots" package of R (http://cran.r-project.org). Circlize package R was used to generate circular heatmap and hierarchical clustering. DESeq was used for normalization. All heatmaps shown are row-normalized for presentation purposes.

Statistics

All data are presented as means ± SEM. Cell culture results consisted of three independent experiments. GraphPad Prism software (GraphPad Software, La Jolla, CA, USA) was used for statistical analysis. *t* test or two-way analysis of variance (ANOVA) with multiple comparisons

(genotype and presence or absence of exercise being the two dependent variables) and Tukey post hoc tests were performed to determine the statistical significance. P values of <0.05 were considered statistically significant.

Study approval

Animal experiments were performed in compliance with the Institutional Animal Care and Use Committee (IACUC) at the UCLA under animal welfare assurance number A3196-01. Both the Veteran Affairs and UCLA IACUC Committees reviewed and approved all animal procedures. The mice colony was housed in the facilities maintained by the Department of Laboratory Animal Medicine, UCLA. Mice obtained from external sources were allowed to acclimate for at least 1 week at UCLA facilities before the start of the experiments.

Supplementary Materials

This PDF file includes:

Supplementary Methods
Figs. S1 to S10
Tables S1 to S3
Legends for tables S4 to S6

Other Supplementary Material for this manuscript includes the following:

Tables S4 to S6

REFERENCES AND NOTES

1. I. A. Tamargo, K. I. Baek, Y. Kim, C. Park, H. Jo, Flow-induced reprogramming of endothelial cells in atherosclerosis. *Nat. Rev. Cardiol.* **20**, 738–753 (2023).
2. J. Lee, P. Fei, R. R. Packard, H. Kang, H. Xu, K. I. Baek, N. Jen, J. Chen, H. Yen, C. C. Kuo, N. C. Chi, C. M. Ho, R. Li, T. K. Hsiai, 4-Dimensional light-sheet microscopy to elucidate shear stress modulation of cardiac trabeculation. *J. Clin. Invest.* **126**, 1679–1690 (2016).
3. P. Silacci, A. Desgeorges, L. Mazzolai, C. Chambaz, D. Hayoz, Flow pulsatility is a critical determinant of oxidative stress in endothelial cells. *Hypertension* **38**, 1162–1166 (2001).
4. J. Hwang, M. H. Ing, A. Salazar, B. Lassegue, K. Griendling, M. Navab, A. Sevanian, T. K. Hsiai, Pulsatile versus oscillatory shear stress regulates NADPH oxidase subunit expression: Implication for native LDL oxidation. *Circ. Res.* **93**, 1225–1232 (2003).
5. T. K. Hsiai, S. K. Cho, P. K. Wong, M. Ing, A. Salazar, A. Sevanian, M. Navab, L. L. Demer, C. M. Ho, Monocyte recruitment to endothelial cells in response to oscillatory shear stress. *FASEB J.* **17**, 1648–1657 (2003).
6. T. K. Hsiai, S. K. Cho, S. Reddy, S. Hama, M. Navab, L. L. Demer, H. M. Honda, C. M. Ho, Pulsatile flow regulates monocyte adhesion to oxidized lipid-induced endothelial cells. *Arterioscler. Thromb. Vasc. Biol.* **21**, 1770–1776 (2001).
7. C. Sasson, R. Eckel, H. Alger, B. Bozkurt, A. Carson, M. Daviglus, P. Deedwania, K. Kirley, C. Lamendola, M. Nguyen, R. Rajgopal Singh, T. Wang, E. Sanchez, American heart association diabetes and cardiometabolic health summit: Summary and recommendations. *J. Am. Heart Assoc.* **7**, e009271 (2018).
8. A. Maass, S. Duzel, M. Goerke, A. Becke, U. Sobieray, K. Neumann, M. Lovden, U. Lindenberger, L. Backman, R. Braun-Dullaeus, D. Ahrens, H. J. Heinze, N. G. Muller, E. Duzel, Vascular hippocampal plasticity after aerobic exercise in older adults. *Mol. Psychiatry* **20**, 585–593 (2015).
9. T. A. Okabe, C. Kishimoto, T. Murayama, M. Yokode, T. Kita, Effects of exercise on the development of atherosclerosis in apolipoprotein E-deficient mice. *Exp. Clin. Cardiol.* **11**, 276–279 (2006).
10. V. L. Aengevaeren, A. Mosterd, S. Sharma, N. H. J. Prakken, S. Mohlenkamp, P. D. Thompson, B. K. Velthuis, T. M. H. Eijsvogels, Exercise and coronary atherosclerosis: Observations, explanations, relevance, and clinical management. *Circulation* **141**, 1338–1350 (2020).
11. A. F. Kramer, K. I. Erickson, S. J. Colcombe, Exercise, cognition, and the aging brain. *J. Appl. Physiol.* **101**, 1237–1242 (2006).
12. L. Mandolesi, A. Polverino, S. Montuori, F. Foti, G. Ferraioli, P. Sorrentino, G. Sorrentino, Effects of physical exercise on cognitive functioning and wellbeing: Biological and psychological benefits. *Front. Psychol.* **9**, 509 (2018).
13. Y. Liu, T. Yan, J. M. Chu, Y. Chen, S. Dunnett, Y. S. Ho, G. T. Wong, R. C. Chang, The beneficial effects of physical exercise in the brain and related pathophysiological mechanisms in neurodegenerative diseases. *Lab. Invest.* **99**, 943–957 (2019).
14. Z. De Miguel, N. Khoury, M. J. Betley, B. Lehallier, D. Willoughby, N. Olsson, A. C. Yang, O. Hahn, N. Lu, R. T. Vest, L. N. Bonanno, L. Yerra, L. Zhang, N. L. Saw, J. K. Fairchild, D. Lee, H. Zhang, P. L. McAlpine, K. Contrepois, M. Shamloo, J. E. Elias, T. A. Rando, T. Wyss-Coray, Exercise plasma boosts memory and dampens brain inflammation via clusterin. *Nature* **600**, 494–499 (2021).
15. J. A. Sanford, C. D. Nogiec, M. E. Lindholm, J. N. Adkins, D. Amar, S. Dasari, J. K. Drugan, F. M. Fernandez, S. Radom-Aizik, S. Schenk, M. P. Snyder, R. P. Tracy, P. Vanderboom, S. Trappe, M. J. Walsh, Molecular Transducers of Physical Activity Consortium, Molecular Transducers of Physical Activity Consortium (MoTrPAC): Mapping the dynamic responses to exercise. *Cell* **181**, 1464–1474 (2020).
16. X. Lu, S. Hu, Y. Liao, J. Zheng, T. Zeng, X. Zhong, G. Liu, L. Gou, L. Chen, Vascular endothelial growth factor B promotes transendothelial fatty acid transport into skeletal muscle via histone modifications during catch-up growth. *Am. J. Physiol. Endocrinol. Metab.* **319**, E1031–E1043 (2020).
17. C. Moessinger, I. Nilsson, L. Muhl, M. Zeitelhofer, B. Heller Sahlgren, J. Skogsberg, U. Eriksson, VEGF-B signaling impairs endothelial glucose transcytosis by decreasing membrane cholesterol content. *EMBO Rep.* **21**, e49343 (2020).
18. T. Kanda, J. D. Brown, G. Orasanu, S. Vogel, F. J. Gonzalez, J. Sartoretto, T. Michel, J. Plutzky, PPARgamma in the endothelium regulates metabolic responses to high-fat diet in mice. *J. Clin. Invest.* **119**, 110–124 (2009).
19. S. Fang, M. C. Livergood, P. Nakagawa, J. Wu, C. D. Sigmund, Role of the peroxisome proliferator activated receptors in hypertension. *Circ. Res.* **128**, 1021–1039 (2021).
20. C. J. Nicol, M. Adachi, T. E. Akiyama, F. J. Gonzalez, PPARgamma in endothelial cells influences high fat diet-induced hypertension. *Am. J. Hypertens.* **18**(PT. 1), 549–556 (2005).
21. L. R. Butcher, A. Thomas, K. Backx, A. Roberts, R. Webb, K. Morris, Low-intensity exercise exerts beneficial effects on plasma lipids via PPARgamma. *Med. Sci. Sports Exerc.* **40**, 1263–1270 (2008).
22. W. C. Man, M. Miyazaki, K. Chu, J. Ntambi, Colocalization of SCD1 and DGAT2: Implying preference for endogenous monounsaturated fatty acids in triglyceride synthesis. *J. Lipid Res.* **47**, 1928–1939 (2006).
23. J. M. Ntambi, M. Miyazaki, Regulation of stearoyl-CoA desaturases and role in metabolism. *Prog. Lipid Res.* **43**, 91–104 (2004).
24. X. Qin, J. Tian, P. Zhang, Y. Fan, L. Chen, Y. Guan, Y. Fu, Y. Zhu, S. Chien, N. Wang, Laminar shear stress up-regulates the expression of stearoyl-CoA desaturase-1 in vascular endothelial cells. *Cardiovasc. Res.* **74**, 506–514 (2007).
25. R. Li, N. Jen, L. Wu, J. Lee, K. Fang, K. Quigley, K. Lee, S. Wang, B. Zhou, L. Vergnes, Y. R. Chen, Z. Li, K. Reue, D. K. Ann, T. K. Hsiai, Disturbed flow induces autophagy, but impairs autophagic flux to perturb mitochondrial homeostasis. *Antioxid. Redox Signal.* **23**, 1207–1219 (2015).
26. K. I. Baek, R. Li, N. Jen, H. Choi, A. Kaboodrangi, P. Ping, D. Liem, T. Beebe, T. K. Hsiai, Flow-responsive vascular endothelial growth factor receptor-protein kinase C isoform epsilon signaling mediates glycolytic metabolites for vascular repair. *Antioxid. Redox Signal.* **28**, 31–43 (2018).
27. H. L. Lujan, H. Janbaih, H. Z. Feng, J. P. Jin, S. E. DiCarlo, Ventricular function during exercise in mice and rats. *Am. J. Physiol. Regul. Integr. Comp. Physiol.* **302**, R68–R74 (2012).
28. H. L. Lujan, S. E. DiCarlo, Cardiac output, at rest and during exercise, before and during myocardial ischemia, reperfusion, and infarction in conscious mice. *Am. J. Physiol. Regul. Integr. Comp. Physiol.* **304**, R286–R295 (2013).
29. S. Madhavan, E. M. C. Kemmerling, The effect of inlet and outlet boundary conditions in image-based CFD modeling of aortic flow. *Biomed. Eng. Online* **17**, 66 (2018).
30. G. Franck, G. Even, A. Gautier, M. Salinas, A. Loste, E. Procopio, A. T. Gaston, M. Morvan, S. Dupont, C. Deschildre, S. Berissi, J. Laschet, P. Nataf, A. Nicoletti, J. B. Michel, G. Caligiuri, Haemodynamic stress-induced breaches of the arterial intima trigger inflammation and drive atherogenesis. *Eur. Heart J.* **40**, 928–937 (2019).
31. K. Ley, Y. Huo, VCAM-1 is critical in atherosclerosis. *J. Clin. Invest.* **107**, 1209–1210 (2001).
32. N. A. Nelken, S. R. Coughlin, D. Gordon, J. N. Wilcox, Monocyte chemoattractant protein-1 in human atheromatous plaques. *J. Clin. Invest.* **88**, 1121–1127 (1991).
33. S. Gencer, B. R. Evans, E. P. C. van der Vorst, Y. Doring, C. Weber, Inflammatory chemokines in atherosclerosis. *Cells* **10**, 226 (2021).
34. M. Orecchioni, K. Kobiyama, H. Winkels, Y. Ghosheh, S. McArdle, Z. Mikulski, W. B. Kiosses, Z. Fan, L. Wen, Y. Jung, P. Roy, A. J. Ali, Y. Miyamoto, M. Mangan, J. Makings, Z. Wang, A. Denn, J. Vallejo, M. Owens, C. P. Durant, S. Braumann, N. Mader, L. Li, H. Matsunami, L. Eckmann, E. Latz, Z. Wang, S. L. Hazen, K. Ley, Olfactory receptor 2 in vascular macrophages drives atherosclerosis by NLRP3-dependent IL-1 production. *Science* **375**, 214–221 (2022).
35. D. A. Towler, M. Bidder, T. Latifi, T. Coleman, C. F. Semenkovich, Diet-induced diabetes activates an osteogenic gene regulatory program in the aortas of low density lipoprotein receptor-deficient mice. *J. Biol. Chem.* **273**, 30427–30434 (1998).
36. D. Huszar, M. L. Varban, F. Rinninger, R. Feeley, T. Arai, V. Fairchild-Huntress, M. J. Donovan, A. R. Tall, Increased LDL cholesterol and atherosclerosis in LDL receptor-deficient mice

with attenuated expression of scavenger receptor B1. *Arterioscler. Thromb. Vasc. Biol.* **20**, 1068–1073 (2000).
37. J. A. Alva, A. C. Zovein, A. Monvoisin, T. Murphy, A. Salazar, N. L. Harvey, P. Carmeliet, M. L. Iruela-Arispe, VE-Cadherin-Cre-recombinase transgenic mouse: A tool for lineage analysis and gene deletion in endothelial cells. *Dev. Dyn.* **235**, 759–767 (2006).
38. S. Kim, H. K. Park, H. Y. Jung, S. Y. Lee, K. W. Min, W. Y. Kim, H. S. Han, W. S. Kim, T. S. Hwang, S. D. Lim, ERG immunohistochemistry as an endothelial marker for assessing lymphovascular invasion. *Korean J. Pathol.* **47**, 355–364 (2013).
39. S. Satta, R. Beal, R. Smith, X. Luo, G. R. Ferris, A. Langford-Smith, J. Teasdale, T. T. Ajime, J. Serre, G. Hazell, G. S. Newby, J. L. Johnson, S. Kurinna, M. J. Humphries, G. Gayan-Ramirez, P. Libby, H. Degens, B. Yu, T. Johnson, Y. Alexander, H. Jia, A. C. Newby, S. J. White, A Nrf2-OSGIN1&2-HSP70 axis mediates cigarette smoke-induced endothelial detachment: Implications for plaque erosion. *Cardiovasc. Res.* **119**, 1869–1882 (2023).
40. Y. Lu, X. Gao, R. Wang, J. Sun, B. Guo, R. Wei, Y. Jia, Adiponectin inhibits proliferation of vascular endothelial cells induced by Ox-LDL by promoting dephosphorylation of Caveolin-1 and depolymerization of eNOS and up-regulating release of NO. *Int. Immunopharmacol.* **73**, 424–434 (2019).
41. J. Vamecq, P. Andreoletti, R. El Kebbaj, F. E. Saih, N. Latruffe, M. H. S. El Kebbaj, G. Lizard, B. Nasser, M. Cherkaoui-Malki, Peroxisomal acyl-CoA oxidase type 1: Anti-inflammatory and anti-aging properties with a special emphasis on studies with LPS and argan oil as a model transposable to aging. *Oxid. Med. Cell. Longev.* **2018**, 6986984 (2018).
42. J. Huang, N. Viswakarma, S. Yu, Y. Jia, L. Bai, A. Vluggens, M. Cherkaoui-Malki, M. Khan, I. Singh, G. Yang, M. S. Rao, J. Borensztajn, J. K. Reddy, Progressive endoplasmic reticulum stress contributes to hepatocarcinogenesis in fatty acyl-CoA oxidase 1-deficient mice. *Am. J. Pathol.* **179**, 703–713 (2011).
43. T. Kubota, N. Kubota, T. Kadowaki, The role of endothelial insulin signaling in the regulation of glucose metabolism. *Rev. Endocr. Metab. Disord.* **14**, 207–216 (2013).
44. T. Kubota, N. Kubota, H. Kumagai, S. Yamaguchi, H. Kozono, T. Takahashi, M. Inoue, S. Itoh, I. Takamoto, T. Sasako, K. Kumagai, T. Kawai, S. Hashimoto, T. Kobayashi, M. Sato, K. Tokuyama, S. Nishimura, M. Tsunoda, T. Ide, K. Murakami, T. Yamazaki, O. Ezaki, K. Kawamura, H. Masuda, M. Moroi, K. Sugi, Y. Oike, H. Shimokawa, N. Yanagihara, M. Tsutsui, Y. Terauchi, K. Tobe, R. Nagai, K. Kamata, K. Inoue, T. Kodama, K. Ueki, T. Kadowaki, Impaired insulin signaling in endothelial cells reduces insulin-induced glucose uptake by skeletal muscle. *Cell Metab.* **13**, 294–307 (2011).
45. X. Sun, H. Lv, P. Zhao, J. He, Q. Cui, M. Wei, S. Feng, Y. Zhu, Commutative regulation between endothelial NO synthase and insulin receptor substrate 2 by microRNAs. *J. Mol. Cell Biol.* **11**, 509–520 (2019).
46. C. W. Tsao, A. W. Aday, Z. I. Almarzooq, A. Alonso, A. Z. Beaton, M. S. Bittencourt, A. K. Boehme, A. E. Buxton, A. P. Carson, Y. Commodore-Mensah, M. S. V. Elkind, K. R. Evenson, C. Eze-Nliam, J. F. Ferguson, G. Generoso, J. E. Ho, R. Kalani, S. S. Khan, B. M. Kissela, K. L. Knutson, D. A. Levine, T. T. Lewis, J. Liu, M. S. Loop, J. Ma, M. E. Mussolino, S. D. Navaneethan, A. M. Perak, R. Poudel, M. Rezk-Hanna, G. A. Roth, E. B. Schroeder, S. H. Shah, E. L. Thacker, L. B. VanWagner, S. S. Virani, J. H. Voecks, N. Y. Wang, K. Yaffe, S. S. Martin, Heart disease and stroke statistics-2022 update: A report from The American Heart Association. *Circulation* **145**, e153–e639 (2022).
47. J. Zhou, Y. S. Li, S. Chien, Shear stress-initiated signaling and its regulation of endothelial function. *Arterioscler. Thromb. Vasc. Biol.* **34**, 2191–2198 (2014).
48. A. J. Brown, Z. Teng, P. C. Evans, J. H. Gillard, H. Samady, M. R. Bennett, Role of biomechanical forces in the natural history of coronary atherosclerosis. *Nat. Rev. Cardiol.* **13**, 210–220 (2016).
49. J. A. Frangos, T. Y. Huang, C. B. Clark, Steady shear and step changes in shear stimulate endothelium via independent mechanisms--superposition of transient and sustained nitric oxide production. *Biochem. Biophys. Res. Commun.* **224**, 660–665 (1996).
50. K. K. Buhman, H. C. Chen, R. V. Farese Jr., The enzymes of neutral lipid synthesis. *J. Biol. Chem.* **276**, 40369–40372 (2001).
51. M. Miyazaki, M. T. Flowers, H. Sampath, K. Chu, C. Otzelberger, X. Liu, J. M. Ntambi, Hepatic stearoyl-CoA desaturase-1 deficiency protects mice from carbohydrate-induced adiposity and hepatic steatosis. *Cell Metab.* **6**, 484–496 (2007).
52. Y. Zou, Y. N. Wang, H. Ma, Z. H. He, Y. Tang, L. Guo, Y. Liu, M. Ding, S. W. Qian, Q. Q. Tang, SCD1 promotes lipid mobilization in subcutaneous white adipose tissue. *J. Lipid Res.* **61**, 1589–1604 (2020).
53. J. M. Ntambi, S. A. Buhrow, K. H. Kaestner, R. J. Christy, E. Sibley, T. J. Kelly Jr., M. D. Lane, Differentiation-induced gene expression in 3T3-L1 preadipocytes. Characterization of a differentially expressed gene encoding stearoyl-CoA desaturase. *J. Biol. Chem.* **263**, 17291–17300 (1988).
54. Y. Zheng, S. M. Prouty, A. Harmon, J. P. Sundberg, K. S. Stenn, S. Parimoo, *Scd3*—A novel gene of the stearoyl-CoA desaturase family with restricted expression in skin. *Genomics* **71**, 182–191 (2001).
55. M. Miyazaki, M. J. Jacobson, W. C. Man, P. Cohen, E. Asilmaz, J. M. Friedman, J. M. Ntambi, Identification and characterization of murine SCD4, a novel heart-specific stearoyl-CoA desaturase isoform regulated by leptin and dietary factors. *J. Biol. Chem.* **278**, 33904–33911 (2003).
56. A. D. Stamatikos, C. M. Paton, Role of stearoyl-CoA desaturase-1 in skeletal muscle function and metabolism. *Am. J. Physiol. Endocrinol. Metab.* **305**, E767–E775 (2013).
57. A. Peter, C. Weigert, H. Staiger, K. Rittig, A. Cegan, P. Lutz, F. Machicao, H. U. Haring, E. Schleicher, Induction of stearoyl-CoA desaturase protects human arterial endothelial cells against lipotoxicity. *Am. J. Physiol. Endocrinol. Metab.* **295**, E339–E349 (2008).
58. A. AM, D. N. Syed, J. M. Ntambi, Insights into stearoyl-CoA desaturase-1 regulation of systemic metabolism. *Trends Endocrinol. Metab.* **28**, 831–842 (2017).
59. K. K. Y. Lai, S. M. Kweon, F. Chi, E. Hwang, Y. Kabe, R. Higashiyama, L. Qin, R. Yan, R. P. Wu, K. Lai, N. Fujii, S. French, J. Xu, J. Y. Wang, R. Murali, L. Mishra, J. S. Lee, J. M. Ntambi, H. Tsukamoto, Stearoyl-CoA desaturase promotes liver fibrosis and tumor development in mice via a Wnt positive-signaling loop by stabilization of low-density lipoprotein-receptor-related proteins 5 and 6. *Gastroenterology* **152**, 1477–1491 (2017).
60. Z. Z. Li, M. Berk, T. M. McIntyre, A. E. Feldstein, Hepatic lipid partitioning and liver damage in nonalcoholic fatty liver disease: Role of stearoyl-CoA desaturase. *J. Biol. Chem.* **284**, 5637–5644 (2009).
61. H. H. Liu, Y. Xu, C. J. Li, S. J. Hsu, X. H. Lin, R. Zhang, J. Chen, J. Chen, D. M. Gao, J. F. Cui, X. R. Yang, Z. G. Ren, R. X. Chen, An SCD1-dependent mechanoresponsive pathway promotes HCC invasion and metastasis through lipid metabolic reprogramming. *Mol. Ther.* **30**, 2554–2567 (2022).
62. J. M. Ntambi, M. Miyazaki, J. P. Stoehr, H. Lan, C. M. Kendziorski, B. S. Yandell, Y. Song, P. Cohen, J. M. Friedman, A. D. Attie, Loss of stearoyl-CoA desaturase-1 function protects mice against adiposity. *Proc. Natl. Acad. Sci. U.S.A.* **99**, 11482–11486 (2002).
63. M. L. MacDonald, M. van Eck, R. B. Hildebrand, B. W. Wong, N. Bissada, P. Ruddle, A. Kontush, H. Hussein, M. A. Pouladi, M. J. Chapman, C. Fievet, T. J. van Berkel, B. Staels, B. M. McManus, M. R. Hayden, Despite antiatherogenic metabolic characteristics, SCD1-deficient mice have increased inflammation and atherosclerosis. *Arterioscler. Thromb. Vasc. Biol.* **29**, 341–347 (2009).
64. G. Jiang, Z. Li, F. Liu, K. Ellsworth, Q. Dallas-Yang, M. Wu, J. Ronan, C. Esau, C. Murphy, D. Szalkowski, R. Bergeron, T. Doebber, B. B. Zhang, Prevention of obesity in mice by antisense oligonucleotide inhibitors of stearoyl-CoA desaturase-1. *J. Clin. Invest.* **115**, 1030–1038 (2005).
65. M. Thurmer, A. Gollowitzer, H. Pein, K. Neukirch, E. Gelmez, L. Waltl, N. Wielsch, R. Winkler, K. Loser, J. Grander, M. Hotze, S. Harder, A. Doding, M. Messner, F. Troisi, M. Ardelt, H. Schluter, J. Pachmayr, O. Gutierrez-Gutierrez, K. L. Rudolph, K. Thedieck, U. Schulze-Spate, C. Gonzalez-Estevez, C. Kosan, A. Svatos, M. Kwiatkowski, A. Koeberle, PI(18:1/18:1) is a SCD1-derived lipokine that limits stress signaling. *Nat. Commun.* **13**, 2982 (2022).
66. J. F. J. Bogie, E. Grajchen, E. Wouters, A. G. Corrales, T. Dierckx, S. Vanherle, J. Mailleux, P. Gervois, E. Wolfs, J. Dehairs, J. Van Broeckhoven, A. P. Bowman, I. Lambrichts, J. A. Gustafsson, A. T. Remaley, M. Mulder, J. V. Swinnen, M. Haidar, S. R. Ellis, J. M. Ntambi, N. Zelcer, J. J. A. Hendriks, Stearoyl-CoA desaturase-1 impairs the reparative properties of macrophages and microglia in the brain. *J. Exp. Med.* **217**, (2020).
67. F. Ascenzi, C. De Vitis, M. Maugeri-Sacca, C. Napoli, G. Ciliberto, R. Mancini, SCD1, autophagy and cancer: Implications for therapy. *J. Exp. Clin. Cancer Res.* **40**, 265 (2021).
68. J. Niebauer, J. P. Cooke, Cardiovascular effects of exercise: Role of endothelial shear stress. *J. Am. Coll. Cardiol.* **28**, 1652–1660 (1996).
69. N. Jen, F. Yu, J. Lee, S. Wasmund, X. Dai, C. Chen, P. Chawareeyawong, Y. Yang, R. Li, M. H. Hamdan, T. K. Hsiai, Atrial fibrillation pacing decreases intravascular shear stress in a New Zealand white rabbit model: Implications in endothelial function. *Biomech. Model. Mechanobiol.* **12**, 735–745 (2013).
70. J. Hong, E. Park, J. Lee, Y. Lee, B. V. Rooney, Y. Park, Exercise training mitigates ER stress and UCP2 deficiency-associated coronary vascular dysfunction in atherosclerosis. *Sci. Rep.* **11**, 15449 (2021).
71. V. L. Li, Y. He, K. Contrepois, H. Liu, J. T. Kim, A. L. Wiggenhorn, J. T. Tanzo, A. S. Tung, X. Lyu, P. H. Zushin, R. S. Jansen, B. Michael, K. Y. Loh, A. C. Yang, C. S. Carl, C. T. Voldstedlund, W. Wei, S. M. Terrell, B. C. Moeller, R. M. Arthur, G. A. Wallis, K. van de Wetering, A. Stahl, B. Kiens, E. A. Richter, S. M. Banik, M. P. Snyder, Y. Xu, J. Z. Long, An exercise-inducible metabolite that suppresses feeding and obesity. *Nature* **606**, 785–790 (2022).
72. H. Chen, C. Chen, M. Spanos, G. Li, R. Lu, Y. Bei, J. Xiao, Exercise training maintains cardiovascular health: Signaling pathways involved and potential therapeutics. *Signal Transduct. Target. Ther.* **7**, 306 (2022).
73. R. M. Evans, G. D. Barish, Y. X. Wang, PPARs and the complex journey to obesity. *Nat. Med.* **10**, 355–361 (2004).
74. Y. Liu, Y. Zhu, F. Rannou, T. S. Lee, K. Formentin, L. Zeng, X. Yuan, N. Wang, S. Chien, B. M. Forman, J. Y. Shyy, Laminar flow activates peroxisome proliferator-activated receptor-gamma in vascular endothelial cells. *Circulation* **110**, 1128–1133 (2004).
75. Y. L. Wang, C. T. Chen, C. S. Tung, M. C. Tsai, Laminar shear stress upregulates the expression of PPARs in vascular endothelial cells under high free fatty acid-induced stress. *Exp. Ther. Med.* **21**, 438 (2021).
76. J. Ikeda, T. Ichiki, Y. Takahara, H. Kojima, C. Sankoda, S. Kitamoto, T. Tokunou, K. Sunagawa, PPARγ agonists attenuate palmitate-induced ER stress through up-regulation of SCD-1 in macrophages. *PLOS ONE* **10**, e0128546 (2015).

77. M. Mukohda, M. Stump, P. Ketsawatsomkron, C. Hu, F. W. Quelle, C. D. Sigmund, Endothelial PPAR-γ provides vascular protection from IL-1β-induced oxidative stress. *Am. J. Physiol. Heart Circ. Physiol.* **310**, H39–H48 (2016).
78. T. M. De Silva, Y. Li, D. A. Kinzenbaw, C. D. Sigmund, F. M. Faraci, Endothelial PPARγ (peroxisome proliferator-activated receptor-γ) is essential for preventing endothelial dysfunction with aging. *Hypertension* **72**, 227–234 (2018).
79. A. M. Beyer, W. J. de Lange, C. M. Halabi, M. L. Modrick, H. L. Keen, F. M. Faraci, C. D. Sigmund, Endothelium-specific interference with peroxisome proliferator activated receptor gamma causes cerebral vascular dysfunction in response to a high-fat diet. *Circ. Res.* **103**, 654–661 (2008).
80. Y. Ma, W. Wang, J. Zhang, Y. Lu, W. Wu, H. Yan, Y. Wang, Hyperlipidemia and atherosclerotic lesion development in Ldlr-deficient mice on a long-term high-fat diet. *PLOS ONE* **7**, e35835 (2012).
81. M. A. Martinez-Gonzalez, C. Sayon-Orea, V. Bullon-Vela, M. Bes-Rastrollo, F. Rodriguez-Artalejo, M. J. Yusta-Boyo, M. Garcia-Solano, Effect of olive oil consumption on cardiovascular disease, cancer, type 2 diabetes, and all-cause mortality: A systematic review and meta-analysis. *Clin. Nutr.* **41**, 2659–2682 (2022).
82. M. A. Carluccio, M. Massaro, C. Bonfrate, L. Siculella, M. Maffia, G. Nicolardi, A. Distante, C. Storelli, R. De Caterina, Oleic acid inhibits endothelial activation. *Arterioscler. Thromb. Vasc. Biol.* **19**, 220–228 (1999).
83. L. Perdomo, N. Beneit, Y. F. Otero, O. Escribano, S. Diaz-Castroverde, A. Gomez-Hernandez, M. Benito, Protective role of oleic acid against cardiovascular insulin resistance and in the early and late cellular atherosclerotic process. *Cardiovasc. Diabetol.* **14**, 75 (2015).
84. D. M. Lee, K. J. Sevits, M. L. Battson, Y. Wei, K. A. Cox-York, C. L. Gentile, Monounsaturated fatty acids protect against palmitate-induced lipoapoptosis in human umbilical vein endothelial cells. *PLOS ONE* **14**, e0226940 (2019).
85. K. A. Harvey, C. L. Walker, Z. Xu, P. Whitley, T. M. Pavlina, M. Hise, G. P. Zaloga, R. A. Siddiqui, Oleic acid inhibits stearic acid-induced inhibition of cell growth and pro-inflammatory responses in human aortic endothelial cells. *J. Lipid Res.* **51**, 3470–3480 (2010).
86. C. A. von Roemeling, L. A. Marlow, J. J. Wei, S. J. Cooper, T. R. Caulfield, K. Wu, W. W. Tan, H. W. Tun, J. A. Copland, Stearoyl-CoA desaturase 1 is a novel molecular therapeutic target for clear cell renal cell carcinoma. *Clin. Cancer Res.* **19**, 2368–2380 (2013).
87. A. Aljohani, M. I. Khan, D. N. Syed, B. Abram, S. Lewis, L. O. Neill, H. Mukhtar, J. M. Ntambi, Hepatic stearoyl-CoA desaturase-1 deficiency-mediated activation of mTORC1- PGC-1α axis regulates ER stress during high-carbohydrate feeding. *Sci. Rep.* **9**, 15761 (2019).
88. F. Romero, X. Hong, D. Shah, C. B. Kallen, I. Rosas, Z. Guo, D. Schriner, J. Barta, H. Shaghaghi, J. B. Hoek, C. Mesaros, A. M. Choi, N. W. Snyder, R. Summer, Lipid synthesis is required to resolve endoplasmic reticulum stress and limit fibrotic responses in the lung. *Am. J. Respir. Cell Mol. Biol.* **59**, 225–236 (2018).
89. M. Ruiz, M. Stahlman, J. Boren, M. Pilon, AdipoR1 and AdipoR2 maintain membrane fluidity in most human cell types and independently of adiponectin. *J. Lipid Res.* **60**, 995–1004 (2019).
90. P. Mukherjee, G. Hough, A. Chattopadhyay, V. Grijalva, E. I. O'Connor, D. Meriwether, A. Wagner, J. M. Ntambi, M. Navab, S. T. Reddy, A. M. Fogelman, Role of enterocyte stearoyl-Co-A desaturase-1 in LDLR-null mice. *J. Lipid Res.* **59**, 1818–1840 (2018).
91. C. Zhu, V. Vedula, D. Parker, N. Wilson, S. Shadden, A. Marsden, svFSI: A multiphysics package for integrated cardiac modeling. *Journal of Open Source Software* **7**, 4118 (2022).
92. T. K. Hsiai, S. K. Cho, H. M. Honda, S. Hama, M. Navab, L. L. Demer, C. M. Ho, Endothelial cell dynamics under pulsating flows: Significance of high versus low shear stress slew rates (d(tau)/dt). *Ann. Biomed. Eng.* **30**, 646–656 (2002).
93. W. Y. Hsieh, K. J. Williams, B. Su, S. J. Bensinger, Profiling of mouse macrophage lipidome using direct infusion shotgun mass spectrometry. *STAR Protoc.* **2**, 100235 (2021).
94. B. Su, L. F. Bettcher, W. Y. Hsieh, D. Hornburg, M. J. Pearson, N. Blomberg, M. Giera, M. P. Snyder, D. Raftery, S. J. Bensinger, K. J. Williams, A DMS shotgun lipidomics workflow application to facilitate high-throughput, comprehensive lipidomics. *J. Am. Soc. Mass Spectrom.* **32**, 2655–2663 (2021).
95. J. J. Mack, T. S. Mosqueiro, B. J. Archer, W. M. Jones, H. Sunshine, G. C. Faas, A. Briot, R. L. Aragon, T. Su, M. C. Romay, A. I. McDonald, C. H. Kuo, C. O. Lizama, T. F. Lane, A. C. Zovein, Y. Fang, E. J. Tarling, T. Q. de Aguiar Vallim, M. Navab, A. M. Fogelman, L. S. Bouchard, M. L. Iruela-Arispe, NOTCH1 is a mechanosensor in adult arteries. *Nat. Commun.* **8**, 1620 (2017).
96. C. Souilhol, B. Tardajos Ayllon, X. Li, M. R. Diagbouga, Z. Zhou, L. Canham, H. Roddie, D. Pirri, E. V. Chambers, M. J. Dunning, M. Ariaans, J. Li, Y. Fang, H. F. Jorgensen, M. Simons, R. Krams, J. Waltenberger, M. Fragiadaki, V. Ridger, S. De Val, S. E. Francis, T. J. Chico, J. Serbanovic-Canic, P. C. Evans, JAG1-NOTCH4 mechanosensing drives atherosclerosis. *Sci. Adv.* **8**, eabo7958 (2022).

Acknowledgments: We wish to express gratitude to S. Reddy (UCLA) and A. Fogelman (UCLA) for providing the *Scd1*$^{floxed/foxed}$; *Ldlr*$^{-/-}$ mice, C. Sigmund (Medical College of Wisconsin) for the EC-DN-PPARγ mice, L. Iruela-Arispe (Northwestern University) for *Cdh5*Cre mice, J. Tidball (UCLA) for providing mouse exercise wheels, and A. Marsden (Stanford University) for the SimVascular Code for CFD analysis. We are grateful for R. McGregor's assistance for the confocal analysis and V. Benavides for assistance with in vitro experiments. **Funding:** This work is supported by Department of Veterans Affairs VA Merit Award I01 BX004356 (T.K.H.) and by National Institutes of Health grants R01HL118650 (T.K.H.) R01HL111437 (T.K.H.), R01HL149808 (T.K.H.), and R35HL144807 (C.D.S). **Author contributions:** Conceptualization: S.C., R.L., and T.K.H. Methodology: S.C., M.R., S.S., J.M.C., and R.L. Software: M.R., S.S., and K.V. Formal analysis: S.C., M.R., and R.L. Investigation: S.C., M.R., S.S., J.M.C., K.I.B., H.P., A.M.B.-M., S.G.-R., J.J.M., and R.L. Resources: C.D.S. and S.T.R. Writing—original draft: S.C., M.R., and T.K.H. Writing—review and editing: S.C., M.R., T.K.H., R.L., S.-K.P., T.Y., J.S., J.J.M., C.D.S., and S.T.R. Visualization: S.C., M.R., and S.S. Funding acquisition: T.K.H. **Competing interests:** The authors declare that they have no competing interests. **Data and materials availability:** All data needed to evaluate the conclusions in the paper are present in the paper and/or the Supplementary Materials. Single-cell RNA sequencing data are available at Dryad (https://datadryad.org/stash/share/FkbIA6PFXt4WMiYMz7ZcD5IOmOJuoZVrs5fzYzo6z84).

Submitted 4 August 2023
Accepted 11 January 2024
Published 14 February 2024
10.1126/sciadv.adj7481